International Journal of Nanomedicine

Dovepress

open access to scientific and medical research

Open Access Full Text Article

ORIGINAL RESEARCH

# Resveratrol-Ampicillin Dual-Drug Loaded Polyvinylpyrrolidone/Polyvinyl Alcohol Biomimic Electrospun Nanofiber Enriched with Collagen for Efficient Burn Wound Repair

Shubham Kanaujiya[1,*], Dilip Kumar Arya[1,*], Prashant Pandey[1], Sneha Singh[2], Giriraj Pandey[1], Shabnam Anjum[3], Md Meraj Anjum[1], Daoud Ali[4], Saud Alarifi[4], Vijayakumar MR[1], Sri Sivakumar[2], Saurabh Srivastava[5], PS Rajinikanth[1]

[1]Department of Pharmaceutical Sciences, Babasaheb Bhimrao Ambedkar University, Lucknow, India; [2]Department of Chemical Engineering, IIT Kanpur, Kanpur, India; [3]Department of Tissue Engineering, School of Intelligent Medicine, China Medical University, Shenyang, Liaoning, 110122, People's Republic of China; [4]Department of Zoology, College of Science, King Saud University, Riyadh, Saudi Arabia; [5]Department of Pharmaceutics, National Institute of Pharmaceutical Education and Research, Hyderabad, Telangana, India

*These authors contributed equally to this work

Correspondence: PS Rajinikanth, Department of Pharmaceutical Sciences, Babasaheb Bhimrao Ambedkar University, Lucknow, India, Email psrajinikanth222@gmail.com

**Background:** The healing of burn wounds is a complicated physiological process that involves several stages, including haemostasis, inflammation, proliferation, and remodelling to rebuild the skin and subcutaneous tissue integrity. Recent advancements in nanomaterials, especially nanofibers, have opened a new way for efficient healing of wounds due to burning or other injuries.

**Methods:** This study aims to develop and characterize collagen-decorated, bilayered electrospun nanofibrous mats composed of PVP and PVA loaded with Resveratrol (RSV) and Ampicillin (AMP) to accelerate burn wound healing and tissue repair.

**Results:** Nanofibers with smooth surfaces and web-like structures with diameters ranging from 200 to 400 nm were successfully produced by electrospinning. These fibres exhibited excellent in vitro properties, including the ability to absorb wound exudates and undergo biodegradation over a two-week period. Additionally, these nanofibers demonstrated sustained and controlled release of encapsulated Resveratrol (RSV) and Ampicillin (AMP) through in vitro release studies. The zone of inhibition (ZOI) of PVP-PVA-RSV-AMP nanofibers against *Staphylococcus aureus* (*S. aureus)* and *Escherichia coli* (*E. coli*) was found 31±0.09 mm and 12±0.03, respectively, which was significantly higher as compared to positive control. Similarly, the biofilm study confirmed the significant reduction in the formation of biofilms in nanofiber-treated group against both *S. aureus* and *E. coli*. X-ray diffraction (XRD) and Fourier transform infrared spectroscopy (FTIR) analysis proved the encapsulation of RSV and AMP successfully into nanofibers and their compatibility. Haemolysis assay (%) showed no significant haemolysis (less than 5%) in nanofiber-treated groups, confirmed their cytocompatibility with red blood cells (RBCs). Cell viability assay and cell adhesion on HaCaT cells showed increased cell proliferation, indicating its biocompatibility as well as non-toxic properties. Results of the in-vivo experiments on a burn wound model demonstrated potential burn wound healing in rats confirmed by H&E-stained images and also improved the collagen synthesis in nanofibers-treated groups evidenced by Masson-trichrome staining. The ELISA assay clearly indicated the efficient downregulation of TNF-alpha and IL-6 inflammatory biomarkers after treatment with nanofibers on day 10.

**Conclusion:** The RSV and AMP-loaded nanofiber mats, developed in this study, expedite burn wound healing through their multifaceted approach.

**Keywords:** electrospinning, nanofiber, resveratrol, ampicillin, burn wound healing, collagen



Received: 21 March 2024
Accepted: 21 May 2024
Published: 7 June 2024

**Graphical Abstract**

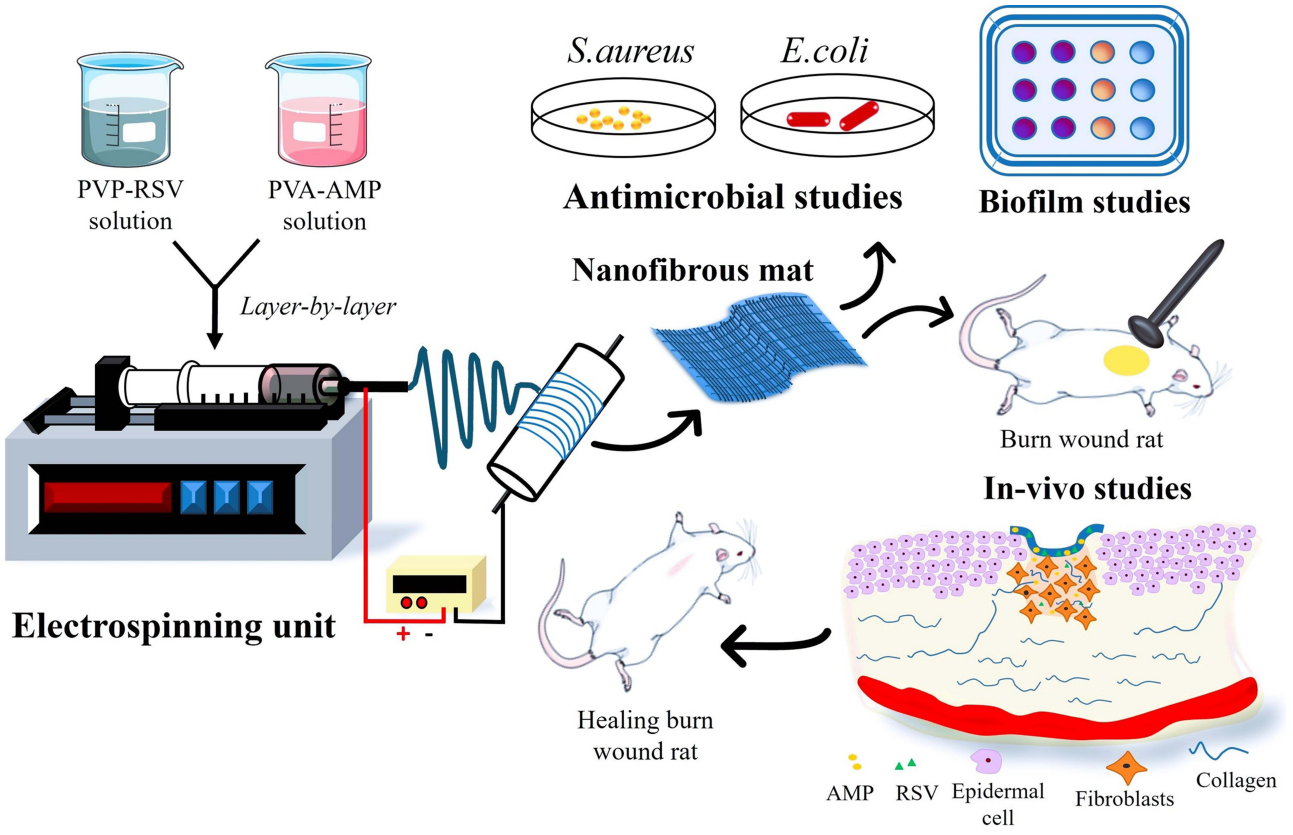


## Introduction

Wounds are classified according to their root cause or mode of administration, such as abrasion, cut, burn, puncture, and others. Because of their complexity, burn wounds are different from surgical and other wounds and necessitate specified, systematic, as well as other local drug delivery considerations.[1–5] Burn injury induces immunosuppression, which renders the patient susceptible to wound infections. Infected burn lesions can progress to chronic wounds, with biofilm making them more difficult to treat.[6] Depending on the depth of the damage, they are classified as first, second, or third-degree wounds. The main issue is the destruction of the skin layers, which serve as a protective barrier against pathogens invasion; as a result, burn patients are much more susceptible to various microbes.[7–10] High temperatures dilate the blood vessels, allowing the liquids contained within to escape and form bubbles, which may cause wounds that are susceptible to infection. In modern burn wound surgery, optimal covering of large burned surfaces remains an intractable problem, putting patients in danger of fatalities or any further disability.[11,12] One possible solution is the development of advanced burn wound healing materials, which could provide effective wound treatment while lowering the risk of complications.[3,13–15]

Nanomaterials for biomedical applications are a new and promising paradigm in biomedical research.[16–19] Nanomaterials with superior physicochemical qualities, biocompatibility, and low biological toxicity can detect local biological conditions and trigger cellular reprogramming to achieve the required therapeutic effectiveness. Nanofibers offer a higher surface-area-to-volume ratio and variable porosity, allowing them to be readily functionalized with biological molecules.[20–23] Nanofibers are nanometre-sized fibre-shaped nanostructures having diameters ranging from 50 to 1000 nm.[24,25] Nanofibers may be made from various polymers and have varying physical characteristics and application possibilities. Because of their distinct biological and physiochemical features, they are employed in health care and biomedical research.[26,27] The sizes of the nanofibers are determined by the kind of polymer employed and the

manufacturing procedure. Electrospinning, initially described in 1934, has been employed for more than 60 years but remains undeveloped in the research of continuous nanofiber manufacturing. Electrospinning is a simple and adaptable technique for producing polymeric nanofibers having diameter nanometres to micrometres, utilizing an electrostatically driven jet of polymeric solution or polymeric melt. Electrospinning forms fibres by applying an electrostatic field to a polymer solution.[28] The process of electrospinning utilizes high voltage to the capillary tip and allows a polymer solution to flow out. Electrospinning is an electrostatic fibre fabrication technique. Electrospinning is a process that spins fibres of diameter ranging from 1 nm to several 1000 nm, producing homogeneous fibres in the nanometre range.[29] Furthermore, electrospinning is an efficient method of loading drugs and antibacterial compounds into the nanofibers composite. Nanofibrous mats have gained considerable interest in the field of wound dressings in tissue repair because of their many benefits, including cost-effectiveness, production ease, large surface area, mechanical properties, high drug encapsulation efficiency, adequate drug loading capacity, multidrug delivery, resemblance with extracellular matrix (ECM), and tunable fibre size, allowing them to absorb exude fluids from the wound surface.

RSV (3, 5, 4′-trihydroxy-trans-stilbene) belongs to the stilbenes category of polyphenols, with two phenyl rings joined by an ethylene bridge. This is a natural polyphenol, identified in over 70 plant species, most notably grape skin and seeds, and has been found in trace levels in red wines as well as other human meals.[30] RSV is a phytoalexin that inhibits the growth of pathogens such as bacteria and fungi. RSV is a potent antioxidant that increases dermal cell proliferation by boosting fibroblast activity and collagen synthesis.[31] RSV also possess anti-inflammatory, anti-ageing, anticancer, anti-diabetic, cardioprotective and neuroprotective properties.[32,33] However, certain potential adverse effects have been identified, including prolonged duration in blood clotting.[34] AMP is a prescription drug which can be used to a wide range of gram-positive and gram-negative bacterial infections including *Staphylococcus aureus* (*S. aureus), Pseudomonas aeruginosa (P.a)* and *Escherichia coli* (*E. coli)*, which are most common in all type of wound infections.[35–37] In vivo administration of AMP has been associated with a spectrum of adverse effects, including gastrointestinal perturbations, hypersensitivity reactions manifesting as cutaneous eruptions, and potential dermatological sequelae.[38] So, the combination of RSV and AMP may enhance the antibacterial activity and would beneficial for reducing drug resistance. The potential synergy between RSV and AMP warrants further investigation. While RSV itself does not possess direct antibacterial activity, it might influence the host's immune response or interact with AMP in a way that could enhance its efficacy against bacterial pathogens.[39,40] Polyvinyl alcohol (PVA) and polyvinylpyrrolidone (PVP) are used to form the nanofiber matrix and enable the nanofibers to have adequate mechanical strength.[41] PVA and PVP are industrial polymers used for various biomedical applications. PVA is well-known for its hydrophilic properties, biocompatibility, and use in the textile industry. PVA melts and degrades quickly in hot solvents. Its major drawback is that it is an unstable solution, and its molecules can recommunicate under physiological conditions; however, blending with PVP can reduce such issues through linkage by H-bond, which raises the blend's stability under physiological conditions. PVP is also known to have good complexing potential.[42] The primary structural protein in the ECM that makes up the many connective tissues of the body is collagen. It makes up between 25% and 30% of the protein in a mammal's whole body and is the basic building block of connective tissue. Collagen plays an important function in wound healing by luring fibroblasts and promoting the deposition of fresh collagen in the wound bed. Collagen dressing promotes autolytic debridement, angiogenesis and re-epithelialization while helping to mimic the formation of new tissue.[43] Recent advancement in electrospinning-based strategies have paved the way to create nanofibrous materials with unique properties for wound dressing applications. Li Y. et al developed advanced electrospun nanoyarn-constructed textile dressing patches of gelatin (Gel)/poly (L-lactic acid) (PLLA) loaded with a Chinese herbal compound (SRHC) for accelerated diabetic wound healing. The SRHC-loaded nanofiber dressing exhibited enhanced therapeutic effects in the diabetic wound healing.[44] Additionally, Zhang C. et al developed silver nanoparticles loaded polyasparthydrazide nanofibrous hydrogel for enhanced healing of full-thickness skin wound. It has demonstrated excellent antibacterial and in-vivo wound healing.[45] To overcome the limitations associated with the conventional therapeutic regime and facilitate accelerated wound healing, we designed the current study to develop collagen decorated bilayered electrospun nanofibrous mat loaded with RSV and AMP for burn wound healing via multifunctional way. The ECM is essential in wound healing because it coordinates epithelialization and angiogenesis. Nanofibers are known to mimic the ECM, and a combination of PVA and PVP at different ratios were used to fabricate

the nanofiber with good stability and mechanical strength. To accelerate the wound healing process further, and to promote tissue regeneration, collagen was additionally decorated with drug loaded nanofiber mats. The developed nanofiber mats were further subjected to different in-vitro and in-vivo characterizations to ensure their potential for burn wound healing.

# Materials and Methods

## Materials

The necessary chemicals for the experiment were sourced from various suppliers. PVA with a molecular weight (M.W.) ranging from 60,000 to 125,000 was obtained from HiMedia Laboratories Pvt. Ltd., Mumbai, India. PVP K-90 with an M. W. of 36,00,00 was purchased from GLR Innovations in New Delhi, India. Beta-cyclodextrin (β-CD) was kindly provided as a gift sample by Ashland Industries in Switzerland. RSV and AMP sodium were acquired from Cayman Chemical Company in the USA and ChemScene in New Jersey, respectively. Finally, collagen was purchased from SRL, Sisco Research Laboratories in India. Dulbecco's modified Eagle's medium (DMEM), antibiotic-antimycotic (100X), fetal bovine serum (FBS), and phosphate buffered saline (PBS 7.4, cell culture grade) were obtained from (Gibco, Life Technologies, USA). All other chemicals and reagents used were of analytical grade. HaCaT cells were received as a kind gift sample from Dr. Sri Sivakumar, Department of Chemical Engineering, IIT Kanpur, India.

## Methods

### Preparation of Polymeric Solutions

PVA 10% (w/v) was dissolved in water and heated to 80°C while being stirred by a magnetic stirrer at 700–800 rpm. Following the preparation of the PVA solution, a separate 0.5% drug (AMP) solution was made in water and combined with PVA solution. A magnetic stirrer formed a clear solution after rapidly stirring 1.5gm of PVP K-90 powder in 13 mL of ethanol. Drug (RSV) and β-cyclodextrin (β-CD) were taken separately in a molecular ratio of 1:2 and dissolved in 2 mL of ethanol to create the drug inclusion complex. Then, the two solutions PVP and RSV- β-cyclodextrin complex were then combined and stirred, yielding 10% w/v as the final concentration of PVP K-90 polymer solution. The required amount of collagen was collected and dissolved in a 0.05 m acetic acid according to the collagen concentration (10 mg/mL).[46]

### Fabrication of Nanofibrous Mat

The layer-by-layer electrospinning technique was used to fabricate the RSV and AMP-loaded PVP/PVA nanofiber mats. About 10 mL of AMP-blended PVA solution was loaded into a 10 mL syringe (22 G) and connected to the electrospinning equipment's syringe pump (E-SPIN Nanotech Super ES-1). The plate collector was encased in aluminum foil to ground the collected fibers. The ideal electrospinning conditions for the AMP-blended PVA solution were 21.1 kV voltage, a flow rate of 0.5 mL/h, and a tip-to-collector distance of 13 cm. The collector plate was covered with a previously prepared AMP-PVA nanofiber layer on aluminum foil.

Then, another 10 mL syringe (20 G) was loaded with 10 mL of the PVP-RSV- β-CD solution and electrospun at 14.6 kV, 0.5 mL/h, and 10 cm tip-to-collector distance.[47] The nanofiber was finally dipped into 10mg/mL of collagen solution for coating. Scheme 1 depicts the methodology for the fabrication of PVA-PVP nanofiber scaffolds encapsulating RSV and AMP. The process involves collagen decoration and crosslinking of the nanofibers.

### Crosslinking of Prepared Nanofiber

Electrospun nanofibrous mats were crosslinked to increase their mechanical properties and stability in varying pH conditions. The nanofiber mat was placed over the 25% glutaraldehyde solution and placed in a sealed desiccator at room temperature for 2 hours after drying in a vacuum for 24 hours. The glutaraldehyde crosslinked mats were vacuum dried after three rounds of distilled water washing. Furthermore, the prepared nanofibers were coated with collagen solution by dipping.[48]

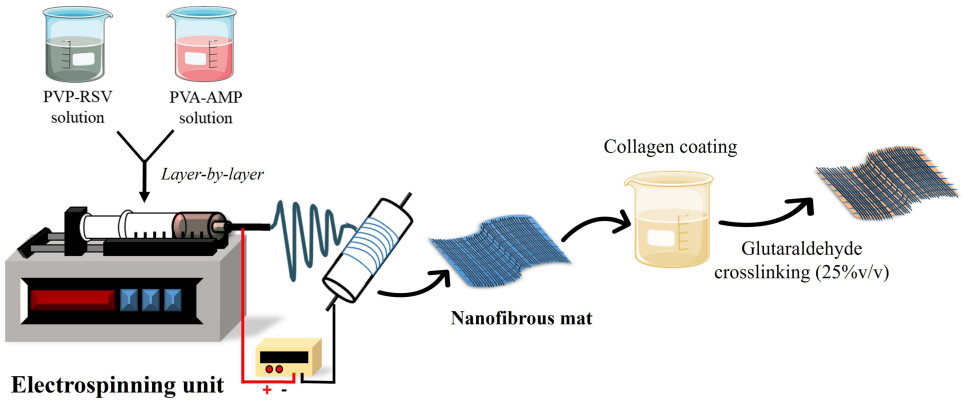


**Scheme 1** Schematic diagram for the preparation of the collagen decorated and crosslinking of PVA-PVP nanofiber scaffolds encapsulated with RSV and AMP.

# Characterizations

## Surface Morphology

Scanning electron microscopy (SEM) (JSM 6490 LV, JEOL) was employed to assess the surface morphology and diameter of the produced nanofibers. Photographs were acquired at 10 kV voltages and then at various fixed magnifications. ImageJ software was used to calculate the average diameter of nanofiber mats at various random positions.[49]

## FTIR Study

FTIR study was performed to detect the structural as well as functional groups of PVA, PVP, RSV, AMP, and PVA-PVP-RSV-AMP nanofiber mats using FTIR of Thermo-Scientific (Nicole 6700). FTIR peaks were obtained at frequencies ranging from 4000 to 400 $cm^{-1}$ to establish drug-excipient compatibility.[50]

## XRD (X-Ray Diffraction)

The crystalline and amorphous characteristics of the synthesized nanofibers were scanned using an X-ray diffractometer (D8 Advance Eco, Bruker, Germany) with a step size of 0.03 within a theta range of 10–60 degrees, and the data were processed.[51]

## Swelling Index

The swelling index was determined by soaking the nanofibers in a phosphate buffer solution (PBS) having pH (7.4) at room temperature. The samples' weight ($W_i$) after cutting into 2 × 2 $cm^2$ was calculated. The samples were then submerged in PBS (pH 7.4), after that, samples from the medium were taken at specific intervals (0, 2, 4, 6, 8, 10, and 12 hours), and any extra water on the surface was soaked up with filter paper.[52,53] The samples' moist weight ($W_f$) was then calculated. Finally, the percentage swelling index was calculated using the following formula.

$$\text{Swelling Index}\,(\%) = \frac{W_f - W_i}{W_f} \times 100$$

## Biodegradability Test

To assess the in-vitro degradation efficacy, the nanofibers were cut into 2 × 2 $cm^2$ and then put into vials containing 4 mg/mL of lysozyme in PBS with a pH of 7.4, followed by incubation at 37°C for varying times. The samples were then taken out of the solution at regular intervals, dried, and weighed after being cleaned with distilled water.[54] The percentage of in-vitro degradation was determined using the ratio of dried sample weight before ($W_i$) and after ($W_f$) deterioration by following equation;

$$\text{Biodegradability}\,(\%) = \frac{W_i - W_f}{W_i} \times 100$$

## In-Vitro Drug Release Study

The nanofiber of RSV and AMP-loaded PVP/PVA was cut into 2 × 2 $cm^2$, and the entrapped drug amount was calculated. The release profile of RSV and AMP-loaded PVA/PVP nanofiber was measured in 10 mL of PBS (pH 7.4) at 37°C and shaking rate of 50 rpm. At predefined time intervals (0, 0.5, 1, 2, 4, 8, 10, 12, 24, 48, 72 and 96 hours), 1 mL sample solution was taken from the dissolution medium, and the same volume of media was reintroduced to maintain the sink state. The calibration curve was utilized to determine the amount of medication released, and the amount of released RSV and AMP was determined using UV spectroscopy at 308 nm and 280 nm wavelengths, respectively. All measurements were done in triplicate, and the findings were reported as mean ± standard deviation.[55,56]

## Antimicrobial Studies

### Zone of Inhibition Test

The agar well disc diffusion technique was used to test the antibacterial efficacy of drug-loaded nanofibers against gram-positive *S. aureus* (ATCC 25923, Seattle, WA, USA) and gram-negative bacteria *E. coli*. *S. aureus* was cultured in tryptone soy broth (TSB) (Himedia LQ508) liquid media for 24 hours at 37°C and 200 rotations per minute. The bacterial cultures were dispersed in triplicate on a Mueller Hinton agar plate (MHA) using a sterile cotton bud stick (Himedia; M173). Under aseptic conditions, a sterile cork borer was used to drill 6 mm holes in the MHA plate. The RSV and AMP-loaded nanofibrous discs with a diameter of 5 mm were cut and sterilized using UV light for 2 hours. Vancomycin was used as a positive control and placebo disc as a negative control. Sterilized discs of positive control, negative control, PVP-RSV, PVA-AMP, and PVP-RSV-PVA-AMP nanofiber mats were placed, and the plates were incubated at 37°C for 24 hours. The antibacterial efficacy was measured and confirmed using a clearly defined zone of inhibition. The experiment was repeated three times, and the average value of the clear zone of inhibition was obtained.[57,58]

### Time Kill Assay

Time-kill assays are useful for determining the time-dependent killing of microbes in the presence of RSV and AMP-loaded nanofibrous mats. The time-kill assay was used to assess the antibacterial activity of RSV and AMP-loaded nanofibers against *S. aureus*. A positive control of 1.0 µg/mL vancomycin was added to a 1 mL culture for *S. aureus* (with a starting inoculum adjusted to 1 × $10^6$ CFU/mL). It should be noted that the antibiotics were given to the positive control culture tubes at sub-MIC concentrations. All the sample tubes were shaken for 24 hours in an orbital shaker at 37°C and 150 revolutions per minute. The colony counts (CFU/mL) were determined at different time intervals (0, 8, and 24 hours) after plating 100 µL dilution factor on a tryptic soy agar plate. CFU (colony forming unit) counts were determined on all plates after incubation, and the experiment was repeated three times for statistically significant results comparing PVP-RSV, PVA-AMP, and PVP-RSV-PVA-AMP nanofiber mats with positive and negative controls.[59]

### Microbial Penetration Test

Pathogenesis begins with the entry of germs into the wound; therefore, the ability of the nanofibrous mats to inhibit microbial infiltration into the wound must be tested. Five 15-mL glass vials were filled with 5 mL of nutritional broth (NB) medium; first vial was covered with cotton ball, second vial was kept open, and three vials were covered with a prepared nanofibrous mat PVP-RSV, PVA-AMP, and PVP-RSV-PVA-AMP, respectively. All of the vials were kept at room temperature for bacterial growth. Bacterial growth was measured in medium-containing vials on days 0, 3, and 7. Positive and negative controls were cotton-plugged and unplugged vials, respectively. Microorganism growth was monitored by determining colony-forming units and using visible spectroscopy at 600 nm.[60]

### Biofilm Formation Assay

*S. aureus* was cultured in tryptic soy broth (TSB-0g) (HiMedia M011), and the strains were grown for 24 hours in the suitable media prior to be diluted 100 times with fresh media and then inoculated in a 96-well microplate in triplicate.[61,62] The 5 mm-diameter nanofibrous mats were punched, subjected to a 2-hour UV sterilization process, and

then incubated in triplicate wells alongside the control groups. Furthermore, the microtiter plates were incubated at 37°C for 24 hours without shaking. The culture was scraped, and the nanofibrous mats were discarded in the following days. The non-adhered cells were washed thrice with PBS pH (7.4) before each well received 150 µL of 95% ethanol for 2 minutes to fix the biofilm. The wells were cleaned three times with 150 µL of PBS pH (7.4) prior to staining for 5 minutes with 150 µL of 1% w/v crystal violet (w/v). In the end, the micro-wells were washed thrice with PBS pH (7.4) and then air-dried and the biofilm intensity was measured at 570 nm using a plate reader.[63]

## Hemolysis Study

The nanofiber samples were cut into 1 × 1 $cm^2$ small pieces for this test, and the blood sample needed for the haemolysis test was drawn from rats and collected in a heparin tube. Nanofiber samples were collected in Eppendorf tubes, diluted with 800 µL (0.9%w/v) sodium chloride solution, and incubated for 30 minutes at 37°C. After 30 minutes, 200µL of blood was injected into each Eppendorf tube. The tubes were shaken and incubated for 30 minutes at 37°C. Deionized water and blood in a ratio of 4:5 was taken as negative controls, while sodium chloride (0.9%w/v) was positive control. The mixture was then collected and centrifuged for 10 minutes at 15,000 rpm. The absorbance of the supernatant was then measured at 540 nm, which indicates destruction of red blood cells (RBCs).[64] The given formula was used to calculate the haemolytic index or percentage of haemolysis.

$$\text{Hemolytic index}\,(\%) = \frac{(\text{Ts} - \text{Nc})}{(\text{Pc} - \text{Nc})} \times 100$$

where Ts, Nc, and Pc denote the absorbance measured for the test sample, negative control, and positive control, respectively.

## Cell Viability Assay

Human keratinocyte (HaCaT) cells were cultured on 1 × 1 $cm^2$ of control, PVP-RSV, PVA-AMP, and PVP-PVA-RSV-AMP nanofiber scaffolds in Dulbecco's Modified Eagle's Medium (DMEM) media containing 10% heat-activated foetal bovine serum (FBS) and 1% antibiotic/antimycotic solution for 5 days. HaCaT cells were grown in 24-well plates, and approximately 1 × $10^5$ cells/well was seeded in each well to perform the cell viability assay. MTT dye at a concentration of (5 mg/mL in PBS) was mixed in each well and incubated for almost 4 hrs. Immediately after the incubation period was over, the MTT dye was removed without disturbing the purple-coloured crystals of formazan. DMSO as a solubilizing agent was added to dissolve the insoluble formazan crystal. Finally, the optical density (OD) at 570 nm was determined to assess the cell viability on day 1, 3 and 5 for all the groups.[65]

## Cell Adhesion and Proliferation on Nanofiber

Cell adhesion was investigated using SEM to visualize the adherence of HaCaT cells to PVP-PVA nanofiber scaffolds containing RSV and AMP on days 1 and 3. The nanofibers, measuring 2 × 2 $cm^2$, were immersed in 70% ethanol for 30 seconds to ensure sterility. Subsequently, they were exposed to ultraviolet (UV) light for 2 hours for sterilization purposes. Following sterilization, 2 × $10^5$ cells/well were seeded onto the nanofibers in 12-well plates and incubated in a $CO_2$ incubator maintained at 37°C with a 5% $CO_2$ atmosphere. After cell fixation with a 4% paraformaldehyde solution for 30 minutes on days 1 and 3, SEM images were captured for analysis.[66]

## In vivo Study

### Animals

The institutional ethics committee approved the animal experimental protocol (approval number RKDF/IAEC /2021/20) and the animals were purchased from the Central Drug Research Institute (U.P.), Lucknow. The in vivo study was conducted on 6–8-week-old Albino Wistar rats weighing approximately 150–200 gm. The animals were housed in polypropylene cages with 12-hour light and 12-hour darkness cycles in normal temperature (23±2°C) and humidity was maintained at 55 ± 5%. A standard laboratory diet (commercial pallet diet) was fed in addition to the drinking water supply. The rats were moved to the laboratory one week before the experiment to acclimatize.

### Wound Closure Study

Ketamine hydrochloride (100 mg/kg body weight) was first used to anaesthetize the animals. Dorsal skin hairs of all the rats were removed using an electric clipper and hair-removing cream. The burn wound was created by inserting a stainless-steel plate into a metal rod (Diameter-1 cm) that had previously been heated on an electric heater for 10 seconds. The wound was cleaned, and all of the formulations were applied directly to the burn area, according to the groups, and the dressing was completed. Changes in the wound area were observed in all groups after treatment at 0, 5, 10, 15 and 21 days. Animals from each group were euthanized on days 5, 10, 15 and 21 for histopathological analysis.[67] The photographs were taken at a specific distance, and the difference in wound closure size was observed. The wound diameter was measured from photographs using the ImageJ software.

### Histopathology

The histopathological examination of the burn wound is generally performed to examine minute changes in tissue structure. Animals from each group were euthanized, and skin/tissue samples containing a portion of the burn wound area were collected on different days (5, 10, 15, and 21) for histological analysis. All the samples were rinsed with saline and stored for 24 hours in a 10% v/v formalin solution. After embedding in paraffin, longitudinal sections (6 µm) were cut utilizing a microtome, and then the sections were stained with Hematoxylin and Eosin (H&E), as well as Masson-trichrome staining for examination under a light microscope.

## ELISA Assay

Estimation of the levels of important pro-inflammatory markers plays an important role in burn wound healing and may be an important parameter of wound healing assessment. Immediately after the burn wound, TNF-α and IL-6 migrate to the wound region and assemble there for a few days, so these inflammatory mediators play a crucial role in the proper healing of the burn wound. For wounds to heal, measuring the expression of inflammatory markers, eg, TNF-α and IL-6 levels, is essential.[68] To determine the level of these mediators, firstly, rats were anesthetized, and the skin of the burn wound was removed on days 0, 7, and 14. Then, in 10:1 normal saline and skin weight was incubated with chilled and sterile normal saline. To create tissue homogenate that was evenly distributed, they were mashed using a high-speed tissue homogenizer. For 15 minutes, the homogenates were centrifuged at 3800 g. Following the recommendations of the manufacturer, filters were used to test the concentrations of TNF-α and IL-6 using an ELISA assay.[69,70]

## Statistical Analysis

All the provided data were represented as mean ± S.D. (standard deviation of mean). GraphPad Prism software version 8.0.1 was used to analyse all the data sets. Statistical comparisons were calculated using one-way ANOVA and followed by means of Bonferroni test for comparison between groups. The $p<0.05$ was considered significant and denoted as *, whereas $p<0.01$ and 0.001 were considered highly significant and represented as ** and ***, respectively.

# Results and Discussion

The electrospinning technique was successfully employed to develop RSV and AMP-loaded PVP/PVA nanofibers by optimising process variables such as voltage, distance between needle and collector, as well as flow rate to get the desired quality product. The nanofibers produced by the optimized process variables and selected concentration of polymers were crosslinked using 25% v/v glutaraldehyde solution. The developed nanofiber scaffolds were further assessed for their in-vitro and in-vivo characteristics suitable for burn wound healing applications.

## Surface Morphology

The surface topography, diameter, and uniformity of the prepared nanofiber were all confirmed by SEM images. The SEM images of the developed PVP/PVA nanofibers showed a uniform diameter and smooth surface, with the diameter ranging from 200 nm to 400 nm. The average diameter of the optimized nanofiber formulations like placebo, F1 (PVP-RSV nanofibers), F2 (PVA-AMP nanofibers), and F3 (PVP-PVA-RSV-AMP nanofibers) were found to be 330.70±31.84 nm, 374.38±56.45 nm, 287.88±50.81nm, and 349.31±73.99 nm, respectively. The developed nanofibers indicated fine,

smooth, and interconnected all-around streamlined nanofibrous mats with web-like porous architecture, as shown in the SEM image (Figure 1A–H), which is considered an ideal property of nanofibers for wound healing applications.

## FTIR Study

The FTIR spectra of PVA, PVP, RSV, AMP, and drug-loaded nanofiber mat (PVP-PVA-RSV-AMP) are presented in Figure 2A. The FTIR analysis of PVP-PVA nanofibers loaded with RSV and AMP reveals the presence of different functional groups in the nanofiber formulation. The peak at 1048 $cm^{-1}$ corresponds to the C-O stretching vibration of PVA, which is a characteristic peak for PVA and confirms the presence of PVA in the nanofiber formulation. The peak at 1368 $cm^{-1}$ corresponds to the C-N stretching vibration of PVP, which confirms the presence of PVP in the nanofiber

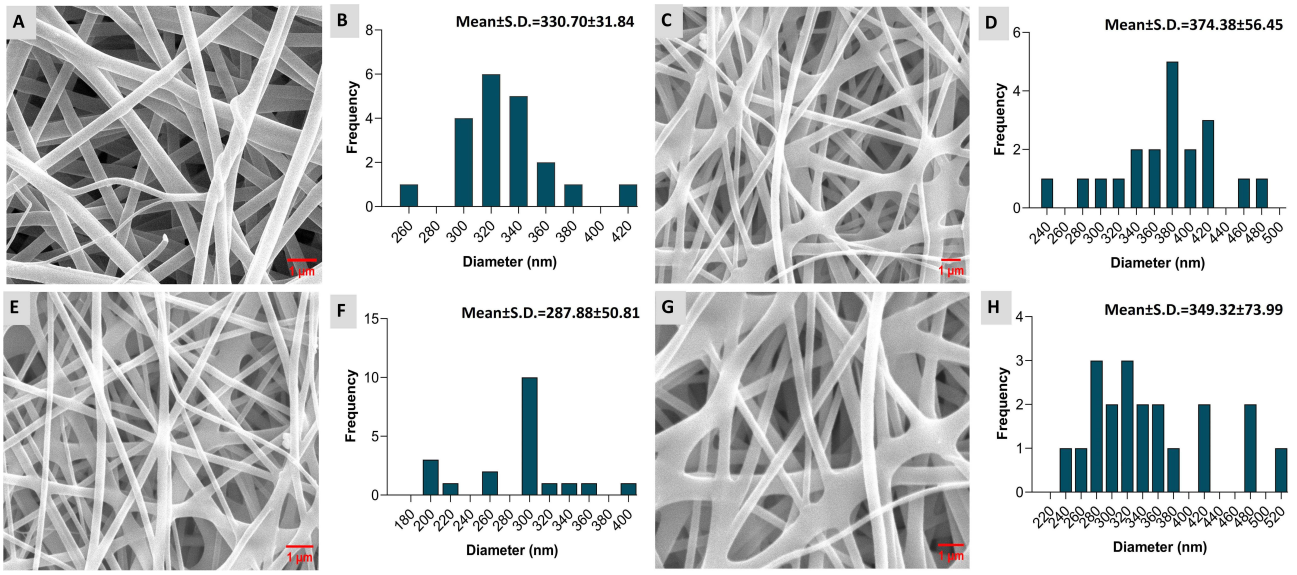


**Figure 1** SEM images and their corresponding average diameter of Placebo (**A** and **B**), PVP-RSV nanofibers (**C** and **D**), PVA-AMP nanofibers (**E** and **F**) and PVP-PVA-RSV-AMP nanofibers (**G** and **H**).

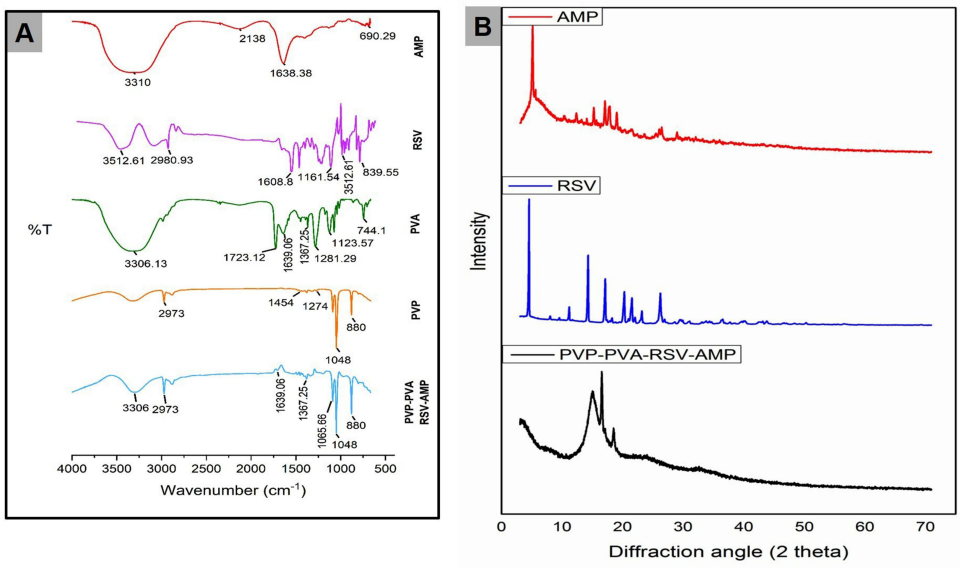


**Figure 2** (**A**) Plot representing FTIR spectra of AMP, RSV, PVA, PVP and drug-loaded nanofiber (PVP-PVA-RSV-AMP) and (**B**) XRD graphs representing the 2θ values of the AMP, RSV and PVP-PVA-RSV-AMP nanofibers.

formulation. The peak at 1639 $cm^{-1}$ corresponds to the amide group (C=O and N-H) of AMP, confirming the presence of AMP in the nanofiber formulation. This peak is essential as it confirms the presence of an antibacterial agent in the nanofibers. The peak at 2973 $cm^{-1}$ corresponds to the C-H stretching vibration of PVP and confirms the presence of PVP in the nanofiber formulation. The peak at 3306 $cm^{-1}$ corresponds to the OH group of RSV, confirming the presence of RSV in the nanofiber formulation. The presence of RSV indicates the potential antioxidant properties of the nanofibers, which could aid in the healing of burn wounds by reducing oxidative stress. Overall, the FTIR analysis confirms the presence of all the functional groups in the nanofiber formulation, suggesting that the PVP-PVA-RSV-AMP nanofibers could be a promising wound dressing material for burn wound healing.

## X-Ray Diffraction (XRD)

The XRD plots of AMP, RSV, and PVP-PVA-RSV-AMP nanofibers are presented in Figure 2B. As per the obtained XRD patterns, both pure RSV and AMP revealed their crystalline nature, AMP showed different peaks at 5.51°, 15.5°, 17.3°, 19.1°, and 26.38°, while RSV revealed distinct peaks at 4.42°, 11.3°,14.44°, 17.7°, 20.41°, 21.76°, and 26.38°. As indicated in Figure 2B, RSV and AMP within the nanofiber formulation are known to change from a crystalline nature to an amorphous or molecular dispersion state.

## Swelling Index

The swelling capacity of nanofiber mats plays an important role in drug loading and release behaviour. The capacity of the developed nanofibers in terms of water absorption and retention was examined to evaluate the volume of exudates that the nanofiber could absorb when applied as a wound dressing. A swelling study was performed for the drug-loaded nanofibers in PBS 7.4 for several time intervals up to 12 hours. The swelling behaviour of different nanofiber formulations is depicted in Figure 3A. PVP-RSV nanofibrous mat showed the highest swelling index (246.62%) during 8 hours as compared to PVA-AMP nanofibrous mat (206.17%) due to the high hydrophilicity of PVP. In the case of PVA-AMP and PVP-PVA-RSV-AMP nanofibrous mat (225.89%), there was a decrease in swelling compared to PVP-AMP because drugs may interact with the polymeric chains and restrict the swelling. After 8 hours, all groups exhibited a decrease in the swelling index. This decrease might be due to the shielding effect of the hydroxyl groups of PVA and carbonyl groups present in PVP. Additionally, polymer

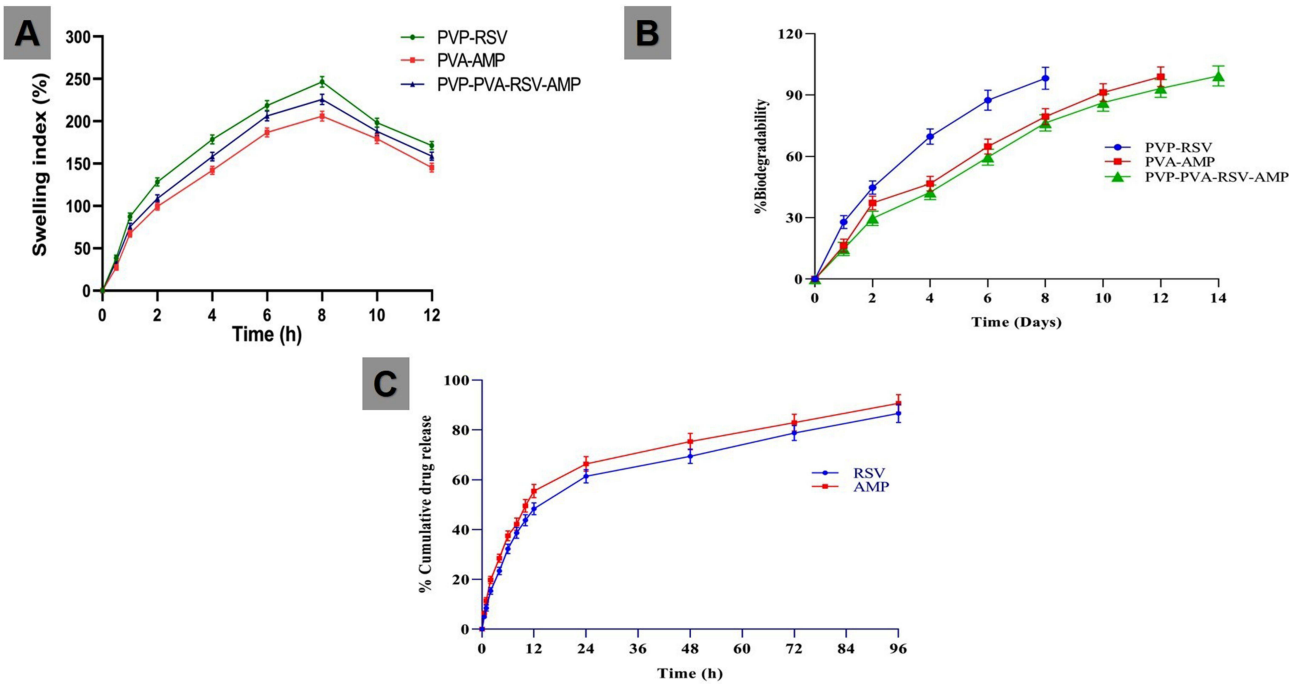


**Figure 3** Graph demonstrating (**A**) swelling index of nanofibers (PVP-RSV, PVA-AMP and PVP-PVA-RSV AMP nanofibers), (**B**) Biodegradability (%) of PVP-RSV, PVA-AMP and PVP-RSV-PVA-AMP nanofibers and (**C**) In-vitro drug release plots of RSV and AMP from PVP-RSV-PVA-AMP nanofiber. All the data represented as mean±SD (n=3).

degradation could also be a factor. The PVA can form intramolecular and intermolecular hydrogen bonds (H-bonds) with each other due to the presence of hydroxyl groups (-OH). When combined with PVP, it forms a strong intermolecular hydrogen bonding between the hydroxyl (OH) group of PVA and the carbonyl (C=O) group of PVP, leading to increased structural stability.

## Biodegradability Test

The in-vitro biodegradation test of the developed nanofibers was performed by immersing the test samples in PBS 7.4, and loss of weight at different time periods was assessed. The results showed that formulation PVP-RSV had degraded by almost 98.26±5.38% on day 8 in PBS 7.4, while the nanofiber PVA-AMP degraded by 98.94±4.78% after 12 days and nanofiber PVP-PVA-RSV-AMP degraded by 99.38±4.85% after 14 days (Figure 3B). The difference was due to the hydrophilic nature of both formulations; the higher the hydrophilicity, the higher the degradation. PVP is more hydrophilic than PVA polymer, that is why the formulation with a combination of PVP/PVA degraded slowly and lasted 14 days, and the formulation with PVP degraded faster than PVA.

## In-Vitro Drug Release Study

The in-vitro drug release of RSV and AMP in nanofibers was determined in PBS (7.4). The PVP-PVA-RSV-AMP formulation exhibited a more sustained and controlled release behaviour as compared to PVP-RSV and PVA-AMP. After 96 hours, the release of RSV and AMP from PVP-RSV-PVA-AMP nanofibers reached 86.68±3.69% and 90.69±3.48%, respectively (Figure 3C). This sustained and controlled release profile suggests that these nanofibers can efficiently deliver drugs to the wound site for an extended period, potentially promoting effective burn wound healing.

## Antimicrobial Study

### Zone of Inhibition Test

Optimised nanofibers were intended to be used in burn wound healing as these wounds are a breeding ground for numerous bacteria. To confirm the ability to protect against microbial infections, PVP-RSV, PVA-AMP, and PVP-PVA-RSV AMP nanofibers were tested against gram-positive and gram-negative bacteria. The antimicrobial activity of nanofiber scaffolds is mentioned in Table 1. The agar disc diffusion method was used in the antimicrobial study against *S. aureus* and *E. coli*. Formation of the zone of inhibition indicates antimicrobial activity; the higher the zone of inhibition, the better the efficacy of the antimicrobial agent. The results obtained from the disc diffusion assay against *S. aureus* and *E. coli* showed that the combination of drugs (PVP-PVA- RSV-AMP nanofibrous mat) produced a maximum zone of inhibition against *S. aureus* (31±0.09 mm) and *E. coli* (12±0.03mm) in comparison to the positive control, negative control, and other single drug-loaded nanofiber formulations as mentioned in Figure 4A–D. The concentration of the drug in the formulation of the nanofibrous mat was found to be directly related to the inhibition zone.

### Microbial Penetration Test

In the microbial penetration assay (Figure 5A), a cotton-plugged vial was used as a negative control revealed some microbial contamination (turbidity) in the vial, an open vial used as a positive control revealed turbidity after 3 days and 7 days, and the drugs-loaded nanofibrous mats (PVP-RSV, PVA-AMP, and PVP-PVA-RSV-AMP) revealed no turbidity due to their antibacterial property. The microbial penetration assay results are graphically represented as a bar diagram in Figure 5B.

**Table 1** Zone of Inhibition Diameter (Mm) of Different Groups Under Study

| Sr. No. | Bacteria | Negative Control | Positive Control | F1 | F2 | F3 |
|---|---|---|---|---|---|---|
| 1. | *Staphylococcus aureus* | 0 | 11.1±0.04 | 14.5±0.05 | 29±0.08 | 31.1±0.09 |
| 2. | *Escherichia coli* | 0 | 10.0±0.03 | 6.5±0.02 | 7.0±0.02 | 12.0±0.03 |

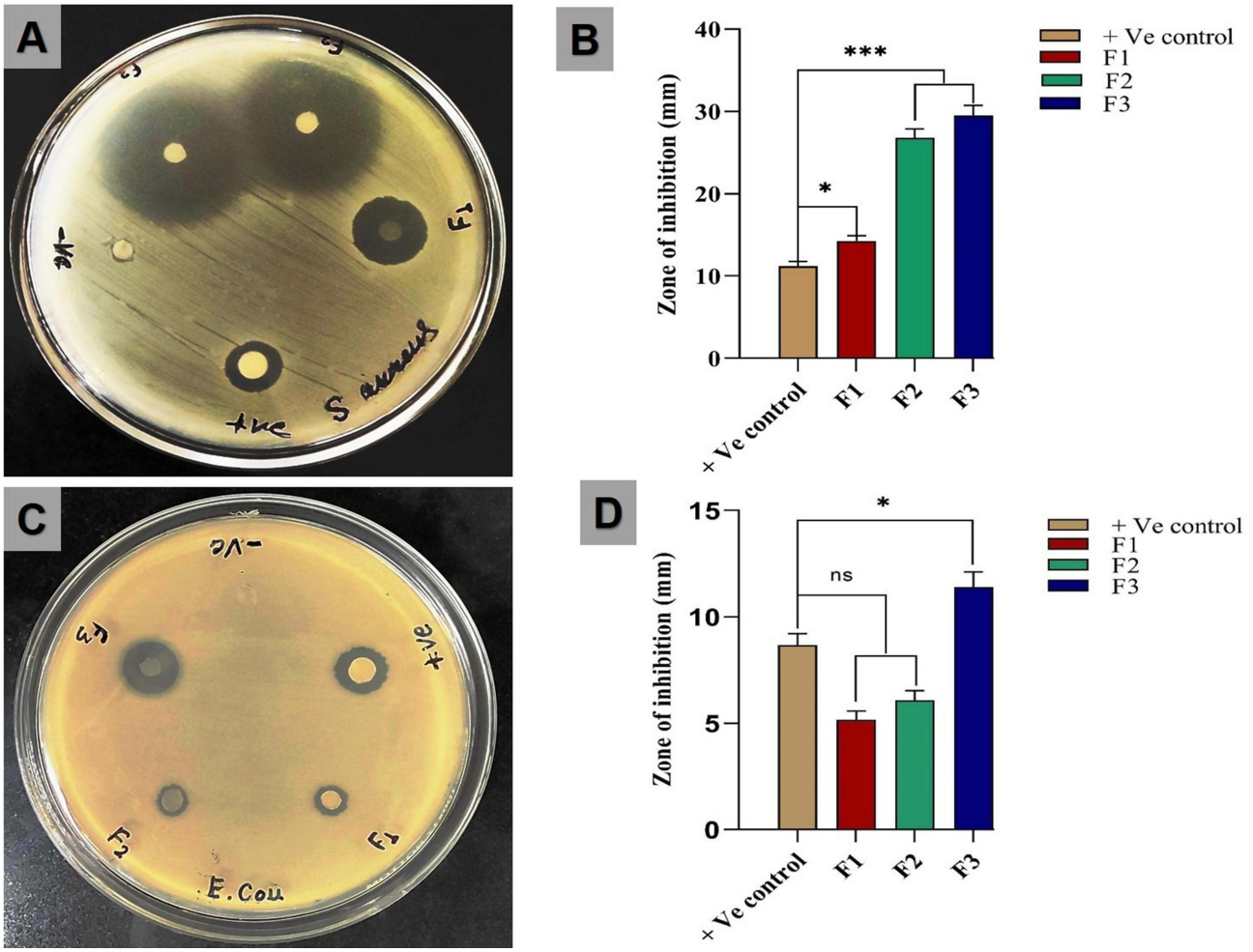


**Figure 4** Plate representing the zone of inhibition against (**A**) *S. aureus* and (**B**) *E.Coli* of positive control, negative control, F1 (PVP-RSV), F2 (PVA-AMP) and F3 (PVP-PVA-RSV-AMP). (**C** and **D**) shows the bar graph of A and B, respectively. *p <0.05, ***p <0.001, one-way ANOVA followed by Bonferroni multiple comparison test. ns denotes non-significant difference between groups. All the data represented as mean±SD (n=3).

## Time Kill Assay

The time-kill assay was used to evaluate the bactericidal activity of drug-loaded nanofibrous mats. The antibacterial activity was found to be time dependent with the use of drug-loaded nanofibrous mats. CFU counts were significantly lower after incubating the nanofibrous mats with *S. aureus* cultures for 0, 8, and 24 hours compared to the positive control (VCM) and *S. aureus* without any drug. The results (Figure 5C) indicate that the PVP-PVA-RSV-AMP nanofibrous mat performs significantly higher bactericidal activity than the PVP-RSV and PVA-AMP nanofibrous mats in killing against *S. aureus* at 8 and 24 hours.

## Biofilm Formation Assay

Biofilm formation assay is an essential parameter for any developed antibacterial regimen to test its efficacy and potency. Biofilms are protective coverings, formed by bacteria in order to neutralize the effects of any antibacterial therapy. In the biofilm formation assay, it was found that *S. aureus* produced biofilm in the TSB-0 g supplemented with 0.5% glucose and the 1% NaCl medium. The culture was incubated with nanofibrous mats loaded with RSV and AMP in 96-well, which significantly reduce the biofilm formation as compared to the control culture as depicted in Figure 6A and B. It was also confirmed in the SEM images of biofilms after treatment with formulation after definite time of culture as given in Figure 6C (i–iv).

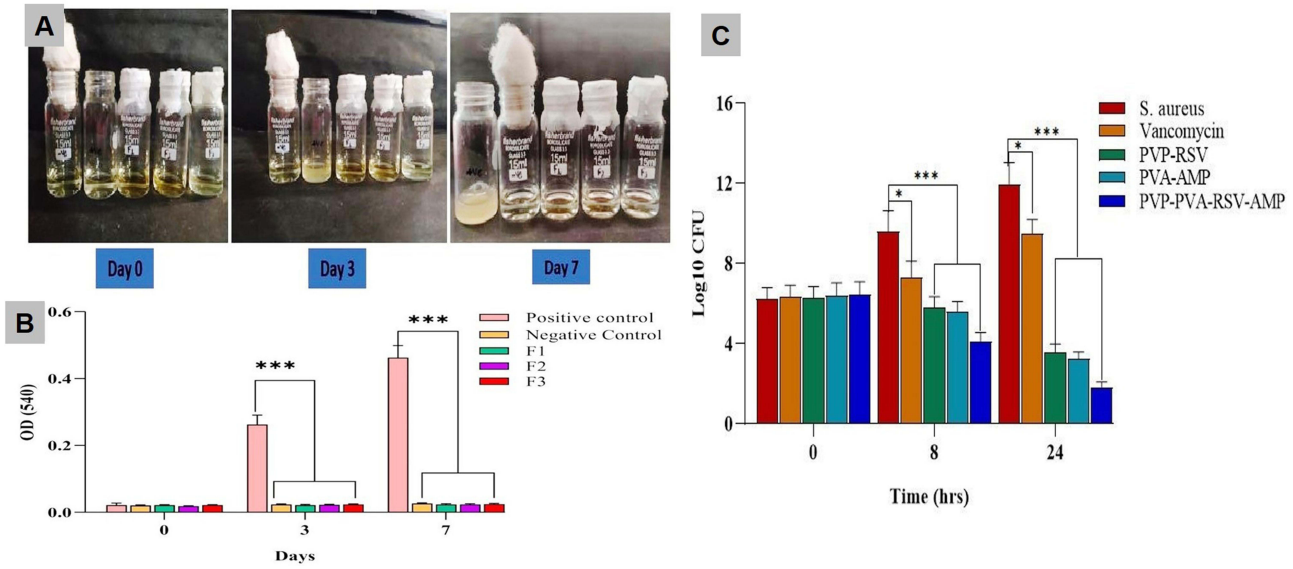


**Figure 5** (**A**) Microbial penetration assay shows Cotton plugged vial as a negative control, Open vial as a positive control, F1 (PVP-RSV), F2 (PVA-AMP) and F3 (PVP-PVA-RSV-AMP) are covered with the drug-loaded nanofibrous mat on 0 day, 3 days, and 7 days. (**B**) Bar diagram representing the optical density of negative control, positive control and the nanofiber samples F1 (PVP-RSV), F2 (PVA-AMP) and F3 (PVP-PVA-RSV-AMP). (**C**) Bar diagram representing the reduction in CFU after-treatment of *S. aureus* with Positive control (VCM), PVP-RSV, PVA-AMP, and PVP-PVA- RSV-AMP nanofiber formulations. *p <0.05, ***p <0.001, one-way ANOVA followed by Bonferroni multiple comparison test. All the data represented as mean±SD (n=3).

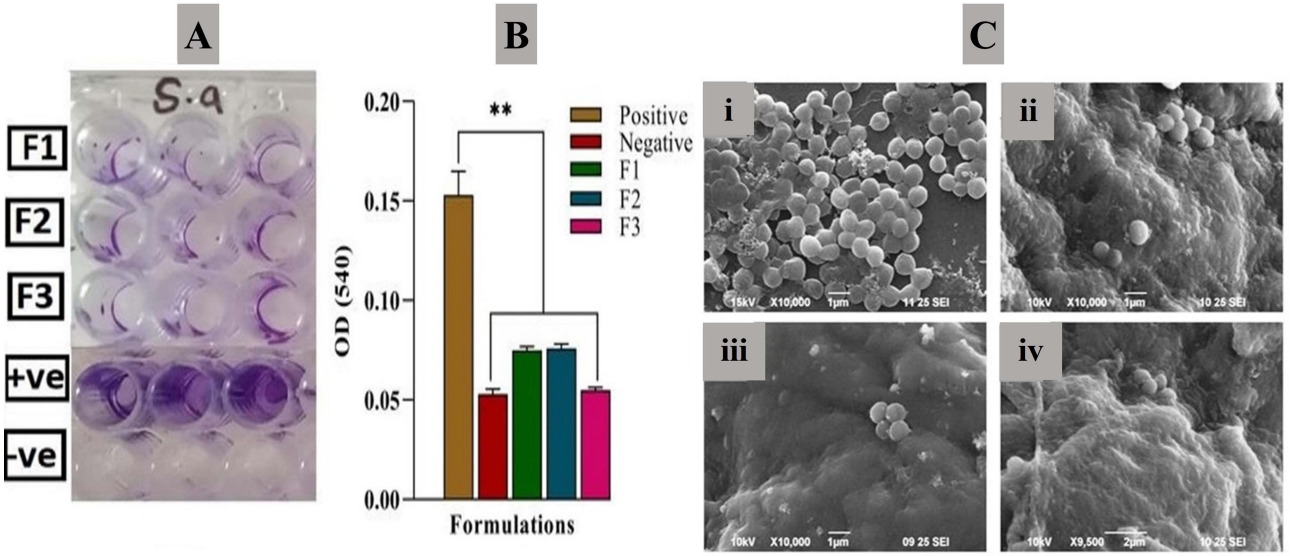


**Figure 6** Effect of various test samples, including drug-loaded nanofibers on the growth of biofilm; (**A**) photograph representing biofilm growth in 96-well plate and (**B**) plot representing a comparative reduction in biofilm after treating with nanofiber formulations. (**C**) SEM images depicting biofilm growth and reduction upon nanofiber treatment of Bacterial film (positive control) (i), Reduction in biofilm after treatment with nanofiber of PVP-RSV (ii), PVA-AMP (iii), and PVP-PVA-RSV-AMP (iv). All the data given as mean±S.D. **p<0.01, one-way ANOVA followed by Bonferroni multiple comparison test. All the data represented as mean±SD (n=3).

## Hemolysis Study

Results of the haemolysis study suggested that the control group's absorbance was higher than the developed nanofiber mats of PVP-RSV, PVA-AMP, and PVP-PVA-RSV-AMP (Figure 7A–C). The haemolytic index of the prepared nanofiber mats was found to be less than 0.3% (Figure 7A and B), and the haemolytic index value less than 5% is considered a non-haemolytic entity. As the haemolytic index of the prepared nanofiber falls within the permissible range, it may therefore be considered non-haemolytic as well as material with better compatibility with blood, indicating a potential alternative for tissue engineering and wound healing applications.

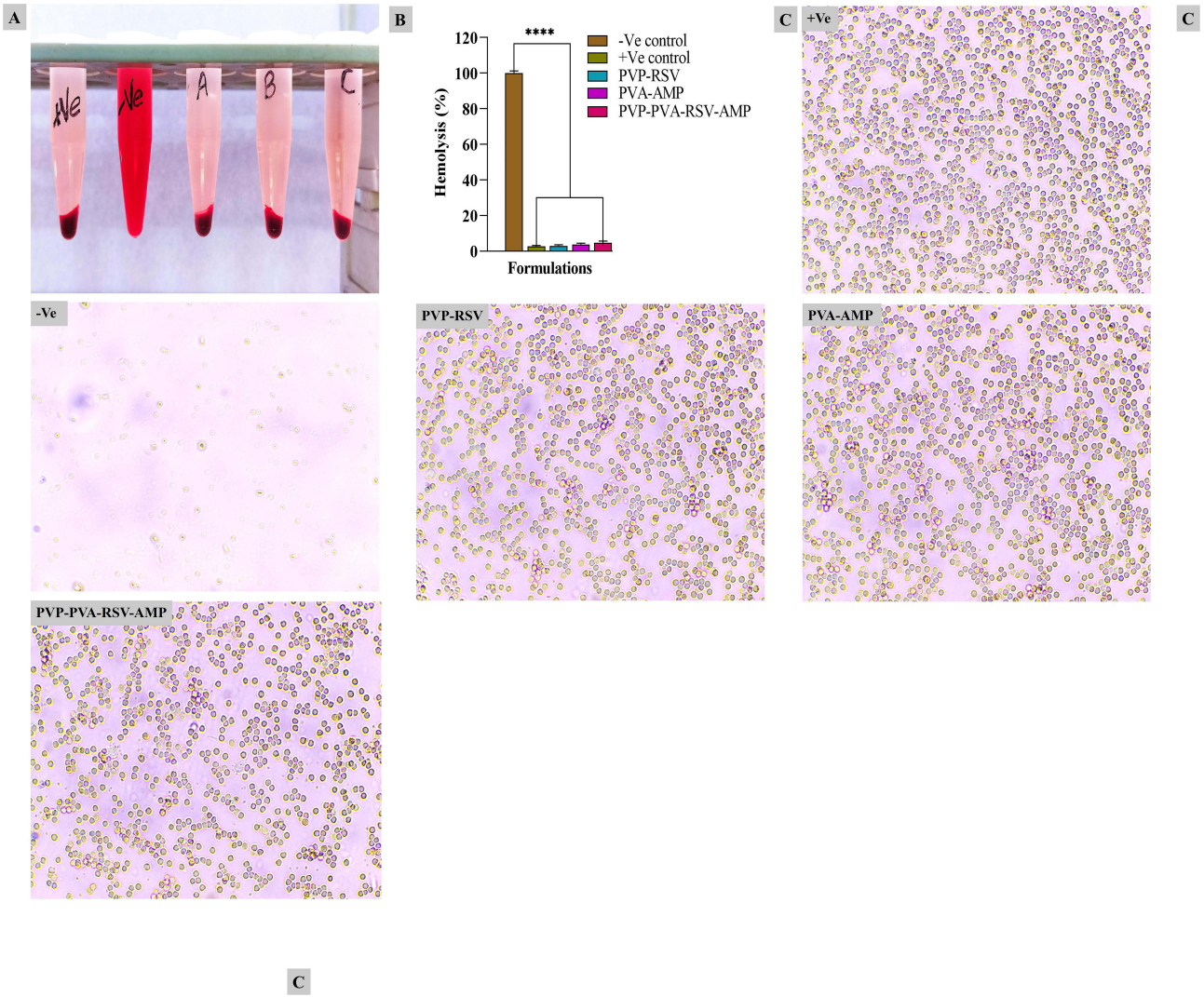


**Figure 7** (**A**) Photograph showing haemolysis of control and nanofiber groups after incubation with RBCs. (**B**) Graph representing their corresponding haemolysis rate (%) of +Ve control, -Ve control, PVP-RSV, PVA-AMP, and PVP-PVA-RSV-AMP nanofibers. (**C**) Microscopic images of RBCs after 30 min of incubation with control and nanofiber groups. ****Represents $p<0.0001$. All the data represented as mean±SD (n=3).

## Cell Viability Assay

Biosafety and biocompatibility are essential properties of any developed formulation. Nanofibers of PVA/PVP loaded with RSV and AMP must satisfy the aforementioned requirements for burn wound healing applications. The cell viability assay was used to confirm the safety of developed nanofibrous scaffolds of RSV and AMP on keratinocytes (HaCaT cells). Figure 8 shows the percentage of cells that survived after day 1, day 3, and day 5 on control, PVP-RSV, PVA-AMP, and PVP-PVA-RSV-AMP nanofibers. The results from Figure 8 confirmed that the percentage cell viability of PVP-RSV, PVA- AMP, and PVP-PVA-RSV-AMP scaffolds was more than 80% on day 1 as compared to control, indicating that developed nanofibers scaffolds are safe and non-toxic and enhance cell proliferation. Similarly on day 3, the percentage cell viability for PVP-RSV, PVA- AMP, and PVP-PVA-RSV-AMP increased significantly as compared to day 1. On day 5, percentage cell viability for PVP-RSV, PVA-AMP, and PVP-PVA-RSV-AMP nanofibers enhanced the cell proliferation of HaCaT cell, clearly indicating its cell growth-promoting capability.

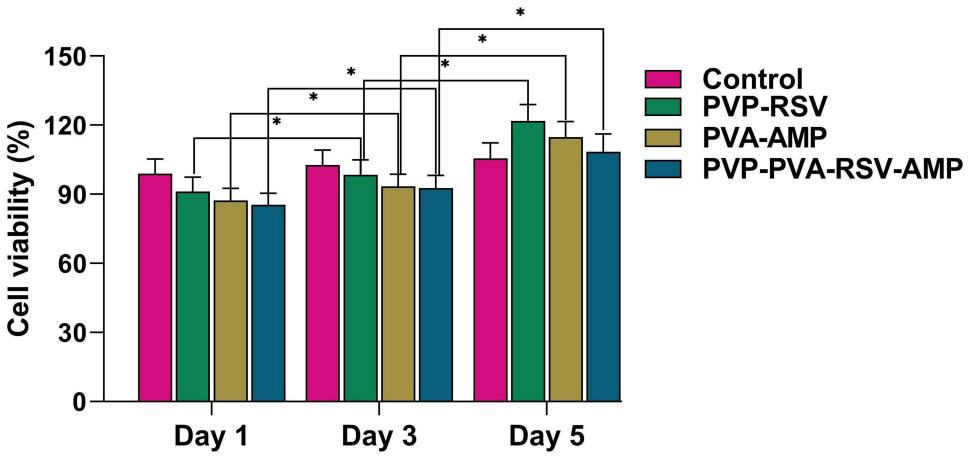


**Figure 8** MTT assay of nanofibrous scaffolds of control, PVP-RSV, PVA- AMP, and PVP-PVA-RSV-AMP nanofibers on HaCaT cell line on day 1, 3 and 5. *p <0.05, one-way ANOVA followed by Bonferroni multiple comparison test. All the data represented as mean±SD (n=3).

## Cell Adhesion

Figure 9 displays the cell adhesion and proliferation of HaCaT cells after treatment with the prepared drug-loaded nanofibers on day 1 and 3. The SEM images (Figure 9A–F) reveal that the seeded cells adhered well to the surface of the scaffolds, underscoring the favourable biocompatibility of the scaffolds. The results also indicate that all tested nanofibers facilitated robust cell adhesion, even after prolonged contact between the nanofibers and HaCaT cells. Notably, PVP-PVA-RSV-AMP exhibited the highest cell adhesion and proliferation behaviour. The cells have effectively enveloped the nanofibrous scaffold, highlighting the importance of aligning the scaffold's structure with the ECM. These observations strongly suggest that the developed nanofibrous scaffolds hold significant potential for promoting burn wound healing and tissue regeneration.[71]

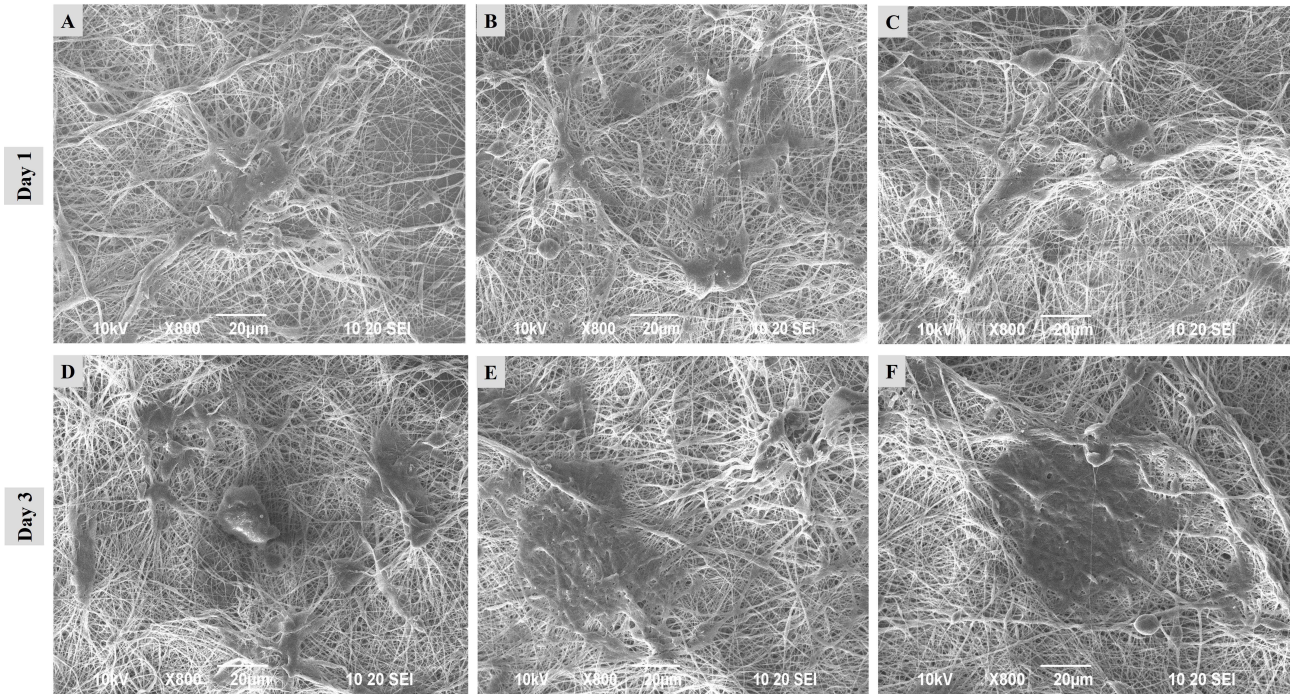


**Figure 9** Cell adhesion of nanofibrous scaffolds of (**A–D**) PVP-RSV, (**B–E**) PVA- AMP, and (**C–F**) PVP-PVA-RSV-AMP nanofibers on HaCaT cell line on day 1 and 3.

# In vivo Studies

## Wound Closure Study

In-vivo studies were performed on a burn wound model involving white albino rats. The in vivo wound closure study results showed that nanofibrous mats containing a combination of RSV and AMP showed accelerated burn wound healing compared to the control groups and other single drug-loaded nanofibrous mats (Figure 10A). It is confirmed that the burn-wound healing effects of PVP-PVA-RSV-AMP nanofibrous mats were remarkably higher as compared to the control, PVP-RSV, and PVA-AMP nanofibrous mats, as the highest wound closure was observed in the group treated with PVP-PVA-RSV-AMP nanofibrous mats. However, after visual observation, marginal changes were observed in the burn-wound size in all experimental groups on different days, and the burn-wound area treated with PVP-PVA-RSV-AMP effectively decreased on 5, 10, 15, and 21 days. Nanofiber formulations were observed to be good mats for burn-wound healing due to properties such as exudate removal, protection from toxic components, prevention of excessive fluid loss, and maintenance of a humid healing environment.[72] The wound area was also calculated using ImageJ software (Figure 10B) and the bar diagram representing the wound area of all the groups on different days (Figure 10C).

## Histopathology Study

The burn-wound healing effect of PVP-RSV, PVA-AMP, and PVP- PVA-RSV-AMP nanofibrous mat was confirmed through histological analysis after 5, 10, 15 and 21 days (Figure 11A) of the wound healing study period. The histopathological changes during the burn wound healing process were evaluated using a light microscope by H&E-stained sections of treatment as well as control groups at days 5, 10, 15, and 21 after creating the burn wound. There were minor differences in the necrotic tissues of control and nanofibers-treated groups on day 5 as the wounds in all groups were found to be highly inflamed. On day 10 and 15, nanofibers-treated groups showed improved re-epithelization and decreased level of necrotic scars as compared to control group. It may be concluded from Figure 11A that nanofibers-

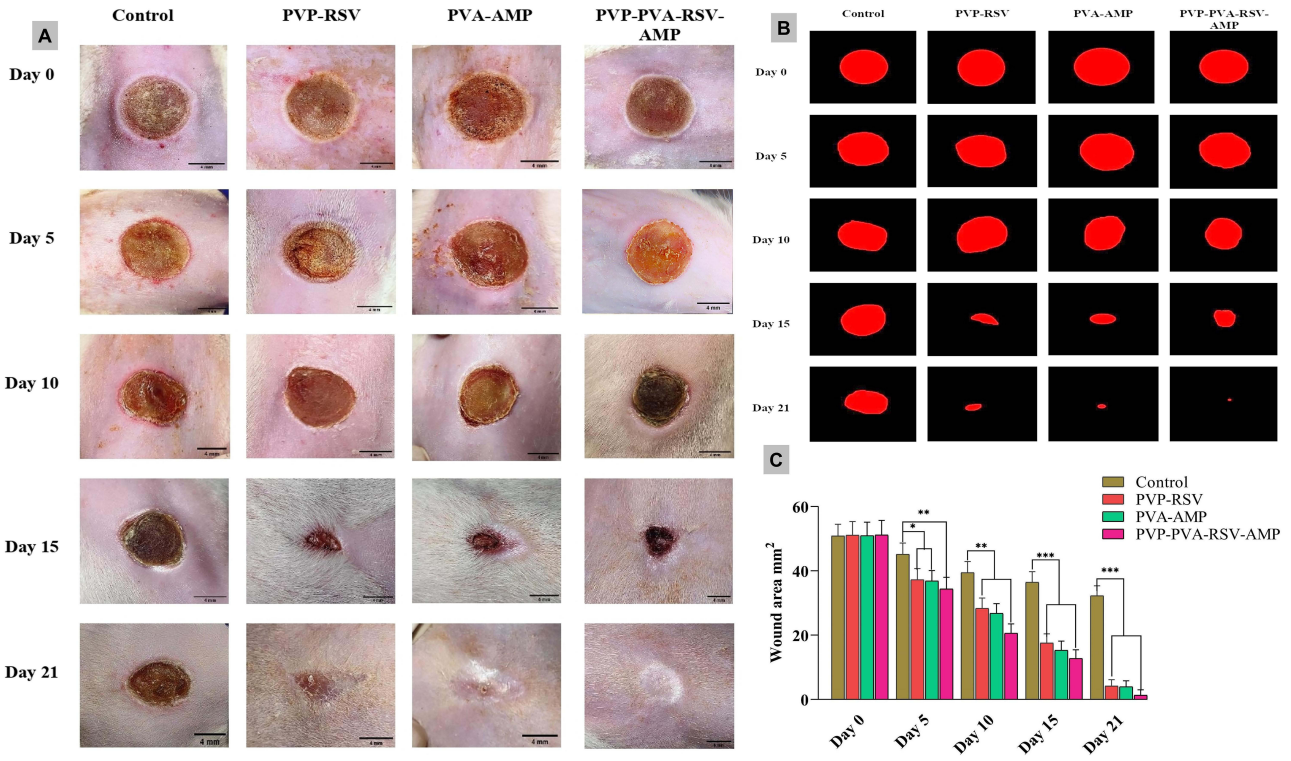


**Figure 10** (**A**) Photographic images representing the burn wound healing of all the groups (Control, PVP-RSV, PVA-AMP, and PVP-PVA-RSV-AMP nanofiber-treated groups) on days 0, 5, 10, 15, and 21, (**B**) Representing the traces of wound area calculated by ImageJ software on different days 0, 1, 5, 10, 15 and 21 and (**C**) Bar diagram representing the % wound area ($mm^2$) after treating the burn wound with drug-loaded nanofibrous mats (PVP-RSV, PVA-AMP, and PVP-PVA-RSV-AMP) and control group. *p <0.05, **p<0.01, and ***p <0.001, one-way ANOVA followed by Bonferroni multiple comparison test. All the data represented as mean±SD (n=3).

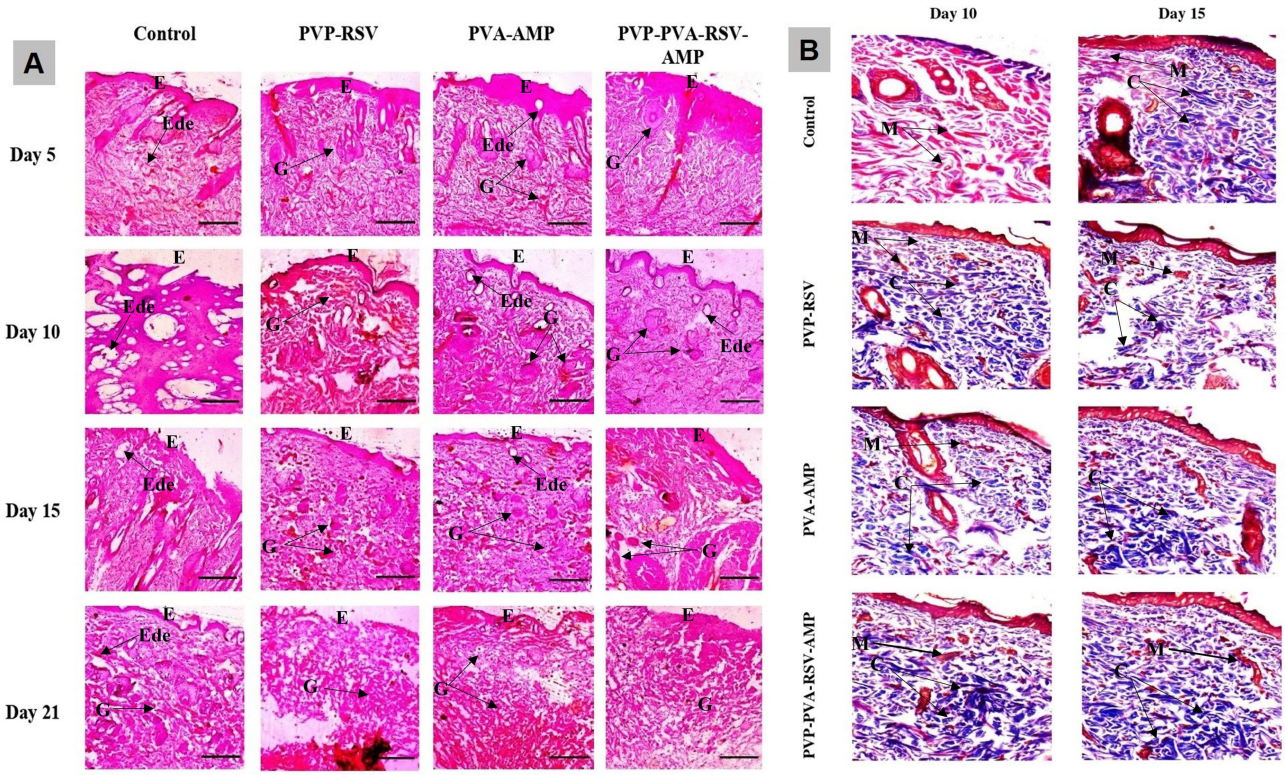


**Figure 11** Histopathology images of (**A**) H&E-stained tissue samples of different groups (Control, PVP-RSV, PVA-AMP, and PVP-PVA-RSV-AMP nanofiber-treated groups) at day 5, 10, 15 and 21, scale bar (50μm). The re-epithelization and granulation in nanofiber-treated groups improved with enhanced fibroblast proliferation and granulation tissue infiltration (E: Epidermis; (G) Granulation tissue; Ede: Edema) and (**B**) Photographs represents the mason-stained histological sections of (Control, PVP-RSV, PVA-AMP, and PVP-PVA-RSV-AMP nanofiber-treated groups) at day 10 and 15 showing the improved collagen formation and maturation (M: Muscle growth in red color; (**C**) Collagen formation in blue color).

treated wounds exhibited the most profound reduction in necrotic scars and inflammation on wound site as compared to control group. It may be due to sufficient hygiene and healing environment provided by nanofibers on wound sites. At day 21, it was observed that the PVP-PVA-RSV-AMP nanofibrous mat treated group showed regeneration of both epithelial and dermal tissues (Figure 11A) more effectively in both area and depth of the burn-wound as compared with the control, PVP-RSV, and PVA-AMP nanofibrous mats. Figure 10B depicts the Masson stained histological images of wound on day 10 and 15 for control and nanofibers-treated groups. Figure 11B clearly indicates the enhanced formation of collagen in nanofibers-treated groups as compared to control. Similarly on day 15, control group showed the immature state of collagen, whereas the nanofibers-treated groups showed improved state of matured collagen. It was confirmed that nanofibers enhanced collagen synthesis and re-epithelization in order to heal burn wounds. Nanofibers may play a critical role in healing burn wounds because they prevent secondary infections. According to the findings, RSV and AMP are likely to prevent secondary infections, proliferate dermal cells, and hasten burn-wound healing.[60] The nanofiber treatment restored wound closure and histological parameters to normal levels. Nanofibers also accelerate wound healing due to their ability to mimic an ECM with a porous structure that allows oxygen to permeate the wounds. Nanofiber has several advantages when used as a wound dressing material as it prevents the infiltration of external infectious agents, and it is biocompatible, biodegradable, and biomimetic, and thus demonstrates accelerated wound healing in rats with burn wounds.[73] The electrospinning technique allows us to cover the wound without requiring multiple dressing changes.

## ELISA Assay

At the site of burn wound, keratinocytes, immediately after burn wound, release cytokines that promote inflammation such as IL-6 and TNF-α, which are important in recruiting and stimulating neutrophils, as evidenced in Figure 12A and B. IL-6 is a crucial cytokine responsible in early inflammation followed by burn injury. IL-6 further enhances the effect of TNF-α, which

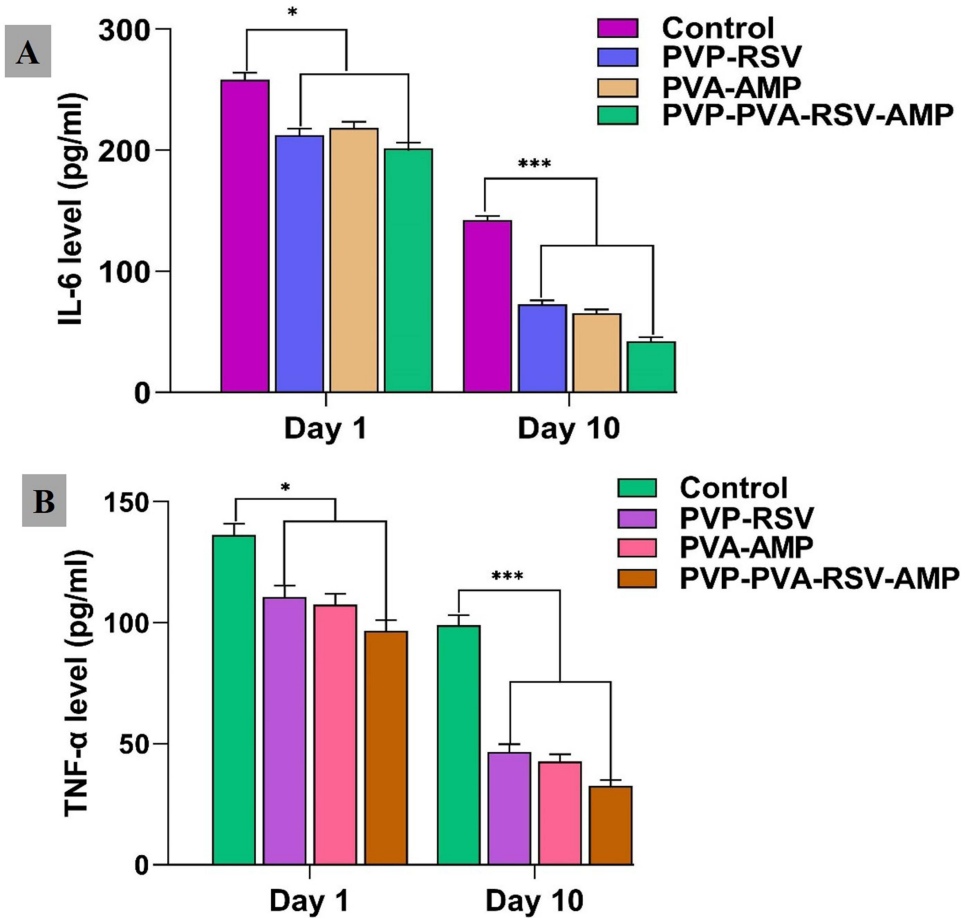


**Figure 12** The level of expression of (**A**) IL-6 and (**B**) TNF-α in control, PVP-RSV, PVA-AMP, and PVP-PVA-RSV-AMP nanofiber-treated groups after day 1 and 10 post treatment. *p <0.05, ***p <0.001, one-way ANOVA followed by Bonferroni multiple comparison test. All the data given as mean±S.D (n=6).

combine to amplify the inflammatory response in the post-burn period. In the burn injury model in rats, it was found from Figure 12 that IL-6 level was significantly higher on day 1 and 10 in the control group when compared to burn wounds of PVP-RSV, PVA-AMP, and PVP-PVA-RSV-AMP nanofiber-treated groups on day 1 and 10. Similarly, the level of TNF-α on days 1 and 10 was also much higher in the control group compared to nanofibers-treated groups on days 1 and 10. This result suggested that the developed RSV and AMP-loaded PVP and PVA nanofibrous scaffolds can efficiently reduce inflammation at the burn wound site and enhance faster wound healing.

## Discussion

Poor wound healing may lead to distressing consequences by increasing the treatment duration, morbidity, and mortality. Antimicrobials and bioactive compounds engaged in appropriate delivery vehicles may be helpful in the effective therapy of burn wounds by decreasing healing time and improving antibiotics efficacy. Quin P. et al developed prohealing peptide RL-QN15 loaded into hollow silica nanoparticles (HSNs) combined with zinc alginate (ZA) gels for chronic wounds management. This peptide-based hydrogel exhibits exceptional hemocompatibility, biocompatibility, and antimicrobial activity, leading to the rapid healing of full-thickness skin wounds and even methicillin-resistant *S. aureus* biofilm-infected chronic wounds in mice.[74] Further, Jia Q. et al prepared a photothermal antibacterial composite hydrogel fabricated with a coating of $Fe^{2+}$ cross-linked carboxymethyl chitosan (FeCMCS) loaded with melanin nanoparticles (MNPs) and the $Cy_{RL\text{-}QN15}$ peptide. The developed hydrogel promoted keratinocyte and fibroblast proliferation while exhibiting high antibacterial efficacy against Gram-positive and Gram-negative bacteria.[75]

Electrospinning technique was employed to develop RSV and AMP-loaded nanofiber mats of PVP and PVA. SEM micrographs revealed that the prepared nanofibers have a smooth, fine interconnected web-like structure and their average diameter falls within 200–400nm, which are the necessary characteristics of nanofibers for application in burn tissue regeneration therapy. The FTIR spectra of polymers, drugs, and fabricated nanofibers showed the physical and chemical compatibility of all with each other. XRD data revealed the amorphous nature of the developed nanofibers, which is important for enhanced drug release in topical formulations. The optimized nanofiber batch presents sufficient biodegradability as well as water retention capacity, which are considered better to absorb the wound exudates on wound site and appropriate for controlled and sustained drug release behaviour required for burn skin tissue regeneration. In-vitro drug release studies established the sustained and controlled release characteristics of nanofiber mats over 96 hrs up to 90%, beneficial for drug delivery for a prolonged period. Antimicrobial studies revealed that prepared nanofibers have significantly improved antibacterial efficacy against both *S. aureus* and *E. coli* as well as anti-biofilm property of these nanofibers against *S. aureus as* compared to standard drugs. Furthermore, in vivo biocompatibility of the nanofibers was confirmed through hemolysis studies on RBCs, demonstrating less than 5% hemolysis, indicative of non-hemolytic behavior. Cell viability assay and cell adhesion on HaCaT cells demonstrated the good cell adhesion and enhanced cell proliferation property of nanofibers. In-vivo study showed excellent burn wound healing potential of nanofibrous scaffolds loaded with RSV and AMP on rats evidenced by H&E and Masson-trichrome staining. Masson-trichrome staining results clearly showed the enhanced collagen formation on day 10 and 15 in nanofiber-treated groups. Significant reduction in pro-inflammatory markers, ie, TNF-α and IL-6, was confirmed by ELISA assay in nanofiber-treated groups compared to control.

## Conclusion

In conclusion, the findings indicate that RSV in combination with AMP has synergistic antimicrobial and burn wound healing activity. The prepared nanofiber mats could potentially be applied as antibacterial wound dressings for prevention and treatment of burn wound infections. According to the findings, the nanofiber formulation developed has excellent properties for burn wound healing in the experimental rats and could be refined for clinical trials in the future. This higher scalability of the developed nanofiber mats sets the stage for novel formulation strategy and commercialization, implying that they may be effective for burn wound healing. Further long-term investigations are warranted to explore its full potential in burn wound treatment.

## Data Sharing Statement

All datasets that support the study are available from the corresponding author on reasonable request.

## Ethics Approval

All animal experiments were approved and supervised by the Ethics Committee of RKDF college of Pharmacy, Bhopal, M.P., India (approval number RKDF/IAEC/2021/20). Animal welfare was ensured according to the Guide for the Care and Use of Laboratory Animals. Since our university's animal ethical committee approval was under evaluation during the work (2020–2021), we applied to our collaborator, RKDF College of Pharmacy, Bhopal, India, and obtained approval for the work in 2021.

## Acknowledgments

This research was supported by Researchers Supporting Project number (RSP2024R27), King Saud University, Riyadh, Saudi Arabia. We also would like to acknowledge RKDF college of Pharmacy, Bhopal, M.P., India for providing animal approval.

## Author Contributions

All authors made a significant contribution to the work reported, whether that is in the conception, study design, execution, acquisition of data, analysis and interpretation, or in all these areas; took part in drafting, revising or critically reviewing the article; gave final approval of the version to be published; have agreed on the journal to which the article has been submitted; and agree to be accountable for all aspects of the work.

## Funding

This research was funded by DST-SERB/SRG project sanctioned under SRG/2019/001273. This research was also funded by GPAT scholarship provided by All India Council for Technical Education (AICTE), India.

## Disclosure

The authors declare no competing interests in this work.

## References

1. Sarhan WA, Azzazy HM, El-Sherbiny IM. Honey/chitosan nanofiber wound dressing enriched with Allium sativum and Cleome droserifolia: enhanced antimicrobial and wound healing activity. *ACS Applied Materials & Interfaces*. 2016;8(10):6379–6390. doi:10.1021/acsami.6b00739
2. Heo DN. Burn-wound healing effect of gelatin/polyurethane nanofiber scaffold containing silver-sulfadiazine. *J Biomed Nanotechnol*. 2013;9 (3):511–515.
3. Yerra A, Dadala MMJJOAPS. Silk fibroin electrospun nanofiber blends with antibiotics and polyvinyl alcohol for burn wound healing. *J Appl Poly Sci*. 2022;139(15):51930.
4. Talukder ME. Novel fibrin functionalized multilayered electrospun nanofiber membrane for burn wound treatment. *J Mat Sci*. 2021;56 (22):12814–12834.
5. Chen S, Liu B, Carlson MA, et al. Recent advances in electrospun nanofibers for wound healing. *Nanomedicine*. 2017;12(11):1335–1352. doi:10.2217/nnm-2017-0017
6. Calum H, Trøstrup H, Laulund AS, et al. Murine burn lesion model for studying acute and chronic wound infections. *APMIS*. 2022;130 (7):477–490. doi:10.1111/apm.13228
7. Guo X, Liu Y, Bera H, et al. α-Lactalbumin-based nanofiber dressings improve burn wound healing and reduce scarring. *ACS Appl Mat*. 2020;12 (41):45702–45713. doi:10.1021/acsami.0c05175
8. Ebrahimi-Hosseinzadeh B. In vivo evaluation of gelatin/hyaluronic acid nanofiber as Burn-wound healing and its comparison with ChitoHeal gel. *Fiber Poly*. 2016;17:820–826.
9. Yergoz F, Hastar N, Cimenci CE, et al. Heparin mimetic peptide nanofiber gel promotes regeneration of full thickness burn injury. *Biomaterials*. 2017;134:117–127. doi:10.1016/j.biomaterials.2017.04.040
10. Alotaibi BS, Khan AK, Ijaz M, et al. Development, characterization, and burn wound-healing potential of neomycin-loaded clay-reinforced nanofibers. *ACS omega*. 2023;8(42):39014–39022. doi:10.1021/acsomega.3c03593
11. Homaeigohar S, Boccaccini ARJAB. Antibacterial biohybrid nanofibers for wound dressings. *Acta Biomaterial*. 2020;107:25–49. doi:10.1016/j.actbio.2020.02.022
12. Hajiali H, Summa M, Russo D, et al. Alginate–lavender nanofibers with antibacterial and anti-inflammatory activity to effectively promote burn healing. *J Mat Chem*. 2016;4(9):1686–1695. doi:10.1039/c5tb02174j
13. Singh R, Roopmani P, Chauhan M, et al. Silver sulfadiazine loaded core-shell airbrushed nanofibers for burn wound healing application. *Int J Pharma*. 2022;613:121358. doi:10.1016/j.ijpharm.2021.121358
14. Li T, Sun M, Wu SJN. State-of-the-art review of electrospun gelatin-based nanofiber dressings for wound healing applications. *Nanomaterials*. 2022;12(5):784. doi:10.3390/nano12050784
15. Sen S, et al. Nanofibers: an effective biomedical tool for burn management. *J Drug Deliv Sci Technol*. 2023;2:104882.
16. Pandey P, Kumar Arya D, Kumar Ramar M, et al. Engineered nanomaterials as an effective tool for HER2+ breast cancer therapy. *Drug Discovery Today*. 2022;27(9):2526–2540. doi:10.1016/j.drudis.2022.06.007
17. Thakor P, Bhavana V, Sharma R, et al. Polymer–drug conjugates: recent advances and future perspectives. *Drug Discovery Today*. 2020;25 (9):1718–1726. doi:10.1016/j.drudis.2020.06.028
18. Reza KK, et al. Biofunctionalized carbon nanotubes platform for biomedical applications. *Mat Lett*. 2014;126:126–130.
19. Kolipaka T, Pandey G, Abraham N, et al. Stimuli-responsive polysaccharide-based smart hydrogels for diabetic wound healing: Design aspects, preparation methods and regulatory perspectives. 2023;324:121537. doi:10.1016/j.carbpol.2023.121537
20. Thakur S, Anjum MM, Jaiswal S, et al. Novel Synergistic approach: tazarotene-calcipotriol-loaded-PVA/PVP-nanofibers incorporated in hydrogel film for management and treatment of psoriasis. *Mole Pharm*. 2023;20(2):997–1014. doi:10.1021/acs.molpharmaceut.2c00713
21. Anand S, et al. Biomaterial-based nanofibers for drug delivery applications. *Biomed Res Med Dis*. 2023;2:531–546.
22. Hashemi -S-S, Saadatjo Z, Mahmoudi R, et al. Preparation and evaluation of polycaprolactone/chitosan/Jaft biocompatible nanofibers as a burn wound dressing. *Burns*. 2022;48(7):1690–1705. doi:10.1016/j.burns.2021.12.009
23. Abid S, Hussain T, Nazir A, et al. Enhanced antibacterial activity of PEO-chitosan nanofibers with potential application in burn infection management. *Int J Biol Macromol*. 2019;135:1222–1236. doi:10.1016/j.ijbiomac.2019.06.022
24. Anjum S, Fabene PF, Mudò G, et al. Electrospun biomimetic nanofibrous scaffolds: a promising prospect for bone tissue engineering and regenerative medicine. *International Journal of Molecular Sciences*. 2022;24(1):23. doi:10.3390/ijms23169206
25. Anjum S, Li T, Arya DK, et al. Biomimetic electrospun nanofibrous scaffold for tissue engineering: preparation, optimization by design of experiments (DOE), in-vitro and in-vivo characterization. *Front Bioeng Biotechnol*. 2023;11:1288539. doi:10.3389/fbioe.2023.1288539
26. Anand S, Pandey, P, Begum, MY, et al. Electrospun biomimetic multifunctional nanofibers loaded with ferulic acid for enhanced antimicrobial and wound-healing activities in STZ-induced diabetic rats. *Pharmaceuticals*. 2022;16(1):15. doi:10.3390/ph15030302
27. Ju HW. Wound healing effect of electrospun silk fibroin nanomatrix in burn-model. *International Journal of Biological Macromolecules*. 2016;85:29–39.
28. Anjum S, Arya DK, Saeed M, et al. Multifunctional electrospun nanofibrous scaffold enriched with alendronate and hydroxyapatite for balancing osteogenic and osteoclast activity to promote bone regeneration. *Front Bioeng Biotechnol*. 2023;11:1302594. doi:10.3389/fbioe.2023.1302594

29. Anand S, Rajinikanth, PS, Arya, DK, et al. Multifunctional biomimetic nanofibrous scaffold loaded with asiaticoside for rapid diabetic wound healing. *Pharmaceutics*. 2022;15(1):14. doi:10.3390/pharmaceutics14020273
30. Vijayakumar MR, Kosuru R, Singh SK, et al. Resveratrol loaded PLGA: d-α-tocopheryl polyethylene glycol 1000 succinate blend nanoparticles for brain cancer therapy. *RSC Advances*. 2016;6(78):74254–74268. doi:10.1039/C6RA15408E
31. Lin Y-C, Hu SC-S, Huang P-H, et al. Electrospun resveratrol-loaded polyvinylpyrrolidone/cyclodextrin nanofibers and their biomedical applications. *Pharmaceutics*. 2020;12(6):552. doi:10.3390/pharmaceutics12060552
32. Shaito A, Posadino AM, Younes N, et al. Potential adverse effects of resveratrol: a literature review. *Int J Mole Sci*. 2020;21(6):2084. doi:10.3390/ijms21062084
33. Annaji M, Poudel I, Boddu SHS, et al. Resveratrol-loaded nanomedicines for cancer applications. *Canc Rep*. 2021;4(3):e1353. doi:10.1002/cnr2.1353
34. Giordo R, Zinellu A, Eid AH, et al. Therapeutic potential of resveratrol in COVID-19-associated hemostatic disorders. *Molecules*. 2021;26(4):856. doi:10.3390/molecules26040856
35. Ghaffari S, Alihosseini F, Rezayat Sorkhabadi SM, et al. Nanotechnology in wound healing; semisolid dosage forms containing curcumin-ampicillin solid lipid nanoparticles, in-vitro, ex-vivo and in-vivo characteristics. *Adv Pharma Bull*. 2018;8(3):395. doi:10.15171/apb.2018.046
36. Mayandi V, Wen Choong AC, Dhand C, et al. Multifunctional antimicrobial nanofiber dressings containing ε-polylysine for the eradication of bacterial bioburden and promotion of wound healing in critically colonized wounds. *ACS Appl Mat*. 2020;12(14):15989–16005. doi:10.1021/acsami.9b21683
37. Li Y. Advances, challenges, and prospects for surgical suture materials. *Acta Biomat*. 2023;1:3.
38. Vincent J-L, et al. Advances in antibiotic therapy in the critically ill. *Critical Care*. 2016;20:1–13.
39. Abedini E. A comprehensive study on the antimicrobial properties of resveratrol as an alternative therapy; 2021.
40. Inchingolo AD. Benefits and implications of resveratrol supplementation on microbiota modulations: a systematic review of the literature. *Int J Mole Sci*. 2022;23(7):4027.
41. Pandey G, Pandey P, Arya DK, et al. Multilayered nanofibrous scaffold of Polyvinyl alcohol/gelatin/poly (lactic-co-glycolic acid) enriched with hemostatic/antibacterial agents for rapid acute hemostatic wound healing. *Int J Pharm*. 2023;638:122918. doi:10.1016/j.ijpharm.2023.122918
42. Mohammed R, Jawad H, Al-Zubiedy A. Blended PVA/PVP Electro spun nanofibers for Coating Application. *Journal of Physics*. 2021:2:4.
43. Rath G, Hussain T, Chauhan G, et al. Collagen nanofiber containing silver nanoparticles for improved wound-healing applications. *J Drug Targ*. 2016;24(6):520–529. doi:10.3109/1061186X.2015.1095922
44. Li Y. Bioactive electrospun nanoyarn-constructed textile dressing patches delivering Chinese herbal compound for accelerated diabetic wound healing. *Mat Des*. 2024;237:112623.
45. Zhang C, Ciasca G, Bonasera A, et al. Electrospun polyasparthydrazide nanofibrous hydrogel loading with in-situ synthesized silver nanoparticles for full-thickness skin wound healing application. *J Photochem Photobiol*. 2024;250:112818. doi:10.1016/j.jphotobiol.2023.112818
46. Yadav S, Arya DK, Pandey P, et al. ECM Mimicking Biodegradable Nanofibrous Scaffold Enriched with Curcumin/ZnO to Accelerate Diabetic Wound Healing via Multifunctional Bioactivity. *Int J Nanomed*. 2022;17:6843–6859. doi:10.2147/IJN.S388264
47. Rahmani F, Ziyadi H, Baghali M, et al. Electrospun PVP/PVA nanofiber mat as a novel potential transdermal drug-delivery system for buprenorphine: a solution needed for pain management. *Applied Sciences*. 2021;11(6):2779. doi:10.3390/app11062779
48. Kamoun EA, Chen X, Mohy Eldin MS, et al. Crosslinked poly (vinyl alcohol) hydrogels for wound dressing applications: a review of remarkably blended polymers. *Arabian Journal of Chemistry*. 2015;8(1):1–14. doi:10.1016/j.arabjc.2014.07.005
49. Agarwal Y, Rajinikanth PS, Ranjan S, et al. Curcumin loaded polycaprolactone-/polyvinyl alcohol-silk fibroin based electrospun nanofibrous mat for rapid healing of diabetic wound: an in-vitro and in-vivo studies. *International Journal of Biological Macromolecules*. 2021;176:376–386. doi:10.1016/j.ijbiomac.2021.02.025
50. Zarei M, Samimi A, Khorram M, et al. Fabrication and characterization of conductive polypyrrole/chitosan/collagen electrospun nanofiber scaffold for tissue engineering application. *Int J Biol Macromol*. 2021;168:175–186. doi:10.1016/j.ijbiomac.2020.12.031
51. Perumal G, Sivakumar PM, Nandkumar AM, et al. Synthesis of magnesium phosphate nanoflakes and its PCL composite electrospun nanofiber scaffolds for bone tissue regeneration. *Mat Sci*. 2020;109:110527. doi:10.1016/j.msec.2019.110527
52. Anjum S, Wang Y, Xin Y, et al. Bioinspired core-shell nanofiber drug-delivery system modulates osteogenic and osteoclast activity for bone tissue regeneration *Materials Today Bio*. 2024;26:101088. doi:10.1016/j.mtbio.2024.101088
53. Saraiva MM, Campelo MDS, Câmara Neto JF, et al. Alginate/polyvinyl alcohol films for wound healing: advantages and challenges. *J BiomedMat Res Part B*. 2023;111(1):220–233. doi:10.1002/jbm.b.35146
54. Song L, Xie X, Lv C, et al. Electrospun biodegradable nanofibers loaded with epigallocatechin gallate for guided bone regeneration. *Composites Part B*. 2022;238:109920. doi:10.1016/j.compositesb.2022.109920
55. Bhattacharya S, Anjum MM, Patel KK. Gemcitabine cationic polymeric nanoparticles against ovarian cancer: formulation, characterization, and targeted drug delivery. *Drug Delivery*. 2022;29(1):1060–1074. doi:10.1080/10717544.2022.2058645
56. Deepak P, Kumar P, Arya DK, et al. c (RGDfK) anchored surface manipulated liposome for tumor-targeted Tyrosine Kinase Inhibitor (TKI) delivery to potentiate liver anticancer activity. *Int J Pharma*. 2023;642:123160. doi:10.1016/j.ijpharm.2023.123160
57. Alven S, Buyana B, Feketshane Z, et al. Electrospun nanofibers/nanofibrous scaffolds loaded with silver nanoparticles as effective antibacterial wound dressing materials. *Pharmaceutics*. 2021;13(7):964. doi:10.3390/pharmaceutics13070964
58. Heunis TD, Smith C, Dicks LMT, et al. Evaluation of a nisin-eluting nanofiber scaffold to treat Staphylococcus aureus-induced skin infections in mice. *Antimicro Agents Chemother*. 2013;57(8):3928–3935. doi:10.1128/AAC.00622-13
59. Chachlioutaki K, Karavasili C, Adamoudi E, et al. Electrospun nanofiber films suppress inflammation in vitro and eradicate endodontic bacterial infection in an e. faecalis-infected ex vivo human tooth culture model. *ACS Biomat Sci Eng*. 2022;8(5):2096–2110. doi:10.1021/acsbiomaterials.2c00150
60. Aljohani MM, Abu-Rayyan A, Elsayed NH, et al. One-pot microwave synthesis of chitosan-stabilized silver nanoparticles entrapped polyethylene oxide nanofibers, with their intrinsic antibacterial and antioxidant potency for wound healing. *Int J Biol Macromole*. 2023;235:123704. doi:10.1016/j.ijbiomac.2023.123704
61. Anjum MM, Patel KK, Dehari D, et al. Anacardic acid encapsulated solid lipid nanoparticles for Staphylococcus aureus biofilm therapy: chitosan and DNase coating improves antimicrobial activity. *Drug Deliv Transl Res*. 2021;11(1):305–317. doi:10.1007/s13346-020-00795-4

62. Patel KK, Surekha DB, Tripathi M, et al. Antibiofilm potential of silver sulfadiazine-loaded nanoparticle formulations: a study on the effect of DNase-i on microbial biofilm and wound healing activity. *Mole Pharm*. 2019;16(9):3916–3925. doi:10.1021/acs.molpharmaceut.9b00527
63. Ramalingam R, Dhand C, Mayandi V, et al. Core–shell structured antimicrobial nanofiber dressings containing herbal extract and antibiotics combination for the prevention of biofilms and promotion of cutaneous wound healing. *ACS Appl Mat*. 2021;13(21):24356–24369. doi:10.1021/acsami.0c20642
64. Bagheri M, Validi M, Gholipour A, et al. Chitosan nanofiber biocomposites for potential wound healing applications: antioxidant activity with synergic antibacterial effect. *Bioeng Transl Med*. 2022;7(1):e10254. doi:10.1002/btm2.10254
65. Park JK, Pham-Nguyen O-V, Yoo HS. Yoo, Coaxial electrospun nanofibers with different shell contents to control cell adhesion and viability. *ACS Omega*. 2020;5(43):28178–28185. doi:10.1021/acsomega.0c03902
66. Soto-Quintero A. Study of the in vitro degradation and characterization of the HaCat keratinocytes adherence on electrospun scaffolds based polyvinyl alcohol/sodium alginate. *J Appl Poly Sci*. 2022;139(39):e52775.
67. Anjum F, Agabalyan NA, Sparks HD, et al. Biocomposite nanofiber matrices to support ECM remodeling by human dermal progenitors and enhanced wound closure. *Scientific Reports*. 2017;7(1):10291. doi:10.1038/s41598-017-10735-x
68. Singh P. Biomimicking dual drug eluting twisted electrospun nanofiber yarns for post-operative wound healing. *Biomed Mat*. 2023;18(3):035006.
69. Thakur S, Anjum MM, Jaiswal S, et al. Tazarotene-calcipotriol loaded Nanostructured lipid carrier enriched hydrogel: a novel dual drug synergistic approach towards Psoriasis management. *J Drug Deliv Sci Technol*. 2023;88:104944. doi:10.1016/j.jddst.2023.104944
70. Jaiswal S, Anjum MM, Thakur S, et al. Evaluation of cardioprotective effect of naringin loaded lignin nanoparticles against isoproterenol induced myocardial infarction. *J Drug Deliv Sci Technol*. 2023;89:105076. doi:10.1016/j.jddst.2023.105076
71. Dutta D, Markhoff J, Suter N, et al. Effect of collagen nanofibers and silanization on the interaction of HaCaT keratinocytes and 3T3 fibroblasts with alumina nanopores. *ACS Appl Bio Mat*. 2021;4(2):1852–1862. doi:10.1021/acsabm.0c01538
72. Fernandes-Cunha GM, Jeong SH, Logan CM, et al. Supramolecular host-guest hyaluronic acid hydrogels enhance corneal wound healing through dynamic spatiotemporal effects. *The Ocular Surface*. 2022;23:148–161. doi:10.1016/j.jtos.2021.09.002
73. de Castro KC, Silva EK, Campos MGN, et al. Hyaluronic acid/polyvinyl alcohol electrospun nanofiber membranes loaded with plantago major extract for smart wound dressings. *ACS Applied Nano Materials*. 2022;5(9):12616–12625. doi:10.1021/acsanm.2c02402
74. Qin P, Tang J, Sun D, et al. Zn2+ cross-linked alginate carrying hollow silica nanoparticles loaded with RL-QN15 peptides provides promising treatment for chronic skin wounds. *ACS Appl Mat*. 2022;14(26):29491–29505. doi:10.1021/acsami.2c03583
75. Jia Q, Fu Z, Li Y, et al. Hydrogel loaded with peptide-containing nanocomplexes: symphonic cooperation of photothermal antimicrobial nanoparticles and prohealing peptides for the treatment of infected wounds. *ACS Appl Mat*. 2024;16(11):13422–13438. doi:10.1021/acsami.3c16061